

A NOVEL PARADIGM OF SENSING:  
MULTI-SIGNALS ACQUISITION WITH ONE SENSOR

A Thesis Submitted to the College of  
Graduate Studies and Research  
In Partial Fulfillment of the Requirements  
For the Degree of Master of Science  
In the Department of Mechanical Engineering  
University of Saskatchewan  
Saskatoon

By

Weijie (Wesley) Shi

© Copyright Weijie Shi, June 2014. All rights reserved.

## PERMISSION TO USE

In presenting this thesis in partial fulfilment of the requirements for a degree of Master of Science from the University of Saskatchewan, I agree that the Libraries of this University may make it freely available for inspection. I further agree that permission for copying of this thesis in any manner, in whole or in part, for scholarly purposes may be granted by the professor or professors who supervised my thesis work or, in their absence, by the Head of the Department or the Dean of the College in which my thesis work was done. It is understood that any copying, publication, or use of this thesis or parts thereof for financial gain shall not be allowed without my written permission. It is also understood that due recognition shall be given to me and to the University of Saskatchewan in any scholarly use which may be made of any material in my thesis.

Requests for permission to copy or to make other use of material in this thesis in whole or part should be addressed to:

Department of Mechanical Engineering

3B48 Engineering Building

57 Campus Drive

Saskatoon, SK S7N 5A9

## ABSTRACT

Sensors with the capability of multi-signal acquisition at the “same” site and “same” time draw abundant attention throughout the academic society. However, designing of multi-signal sensors is a challenging process. The goal of the study is to explore the design theories and methodologies for multi-signal sensors with current device manufacturing technologies. To achieve this goal, this study strives to meet the following two objectives: (1) define general design principles for such sensors, and (2) develop demonstration prototypes to prove the effectiveness of the design principle. The study takes two signals acquisition as a vehicle without loss of generality.

For Objective 1, this study proposes three general design principles for multi-signal sensors. The first design principle is to acquire multiple signals through a stem signal. The second principle is to design the structure so that one signal can be accurately inferred while another signal can be directly measured. The third principle is to design an integral structure that inherently acquires two signals. For objective 2, prototypes for the second and third principles were built to demonstrate the effectiveness of the design principles.

Contributions of this study to the field of composite materials and sensor design include: (1) findings of the three design principles for multi-signal acquisition, (2) proof-of-concept construction/application of two prototype multi-signal devices (one for temperature and pressure, and the other for temperature and pH), and (3) discovery of the highly linear relationship between the temperature and electrical resistivity with a carbon nanotube and polymer composite within the temperature range from room temperature to approximately 70 Celsius degrees.

## ACKNOWLEDGMENTS

At first, I am truly grateful for the relentless help and support from my supervisor, Dr. W.J. (Chris) Zhang. Throughout my study at the U of S, he has provided me with his unique perspective and advice, and guided me out of a swath of mists when I was stumped by many conundrums. Even during the darkest moment of my life, I was still able to stick to it as he told me that every cloud has a silver lining. As here I am, on the verge of graduation, when all the effort I have spent is about to be rewarded. I would like to thank him again for everything that he has done; an important and irreplaceable trail on my university life.

I would also like to extend my sincere gratitude to my co-supervisor, Li Chen, and the fellow technicians in the Department of Electrical Engineering, who have offered their assistance in assembling and gathering all the electrical devices for my experiments.

My special thanks are paid to the China Scholarship Council for their four-year financial support to my research.

Last but not the least; I would like to thank the following personnel: Dr. KI-Young Song, Dr. Miao Yu, and Dr. R. Sammynaiken for their continuous academic assistance and advice, Dr. R. Sammynaiken's hospitable and selfless help in preparing the experiment bench, materials, and equipment. For all the others who have not been mentioned, you have my acknowledgement.

## DEDICATION

This thesis is dedicated to my Mum and Dad, and to everyone who has supported me all along. My work could not have been completed without you.

## TABLE OF CONTENTS

	<u>page</u>
PERMISION TO USE .....	i
ABSTRACT .....	ii
ACKNOWLEDGMENTS .....	iii
DEDICATION .....	iv
TABLE OF CONTENTS.....	v
LIST OF TABLES .....	vii
LIST OF FIGURES .....	viii
LIST OF ABBREVIATIONS.....	x
CHAPTER 1 .....	1
1.1    Motivation.....	1
1.2    Research Problem .....	2
1.3    Research Objectives and Scope .....	4
1.4    Overview of Methodology .....	4
1.5    The Organization of the Thesis.....	5
CHAPTER 2 .....	7
2.1    Preliminary Concept .....	7
2.2    Sensor Technology Developments Related to OSMS .....	8
2.2.1    The Work of Lin’s Group .....	8
2.2.2    Fiber Bragg Grating Sensor for Temperature and Strain Measurement .....	9
2.2.3    Magneto-elastic Micro-Sensor Array .....	11
2.2.4    Thin Film Technology for Multi-signal Acquisition .....	12
2.3    Concluding Remarks.....	15
CHAPTER 3 .....	16
3.1    Principle 1: Acquiring Multiple Signals through a Stem Signal.....	16
3.2    Principle 2: One Signal Inference and One Signal Measurement.....	17
3.3    Principle 3: Acquiring Multiple Signals through a Multi-transducer Structure .....	18
CHAPTER 4 .....	21
4.1    A Pipe System for Temperature and Pressure Measurement.....	21
4.2    Temperature Inference Model Development .....	25

4.3	Experiment Setup.....	28
4.3.1	Data Acquisition System.....	28
4.3.2	Test Bed .....	32
4.4	Results and Analysis .....	34
4.5	Conclusion .....	38
CHAPTER 5 .....		39
5.1	Temperature Measurement with CNT Films .....	39
5.2	pH-value Measurement with the CNT Films.....	50
5.2.1	PANI-CNT Film Preparation.....	50
5.2.2	pH-value and Temperature Measurement.....	53
5.3	Temperature Dependence of the CNT Film without PANI: Discussion .....	56
5.4	Sensitivity of the PANI-CNT film to pH: Discussion .....	61
5.5	Conclusion .....	61
CHAPTER 6 .....		62
6.1	Overview and Conclusion.....	62
6.2	Contributions.....	63
6.3	Future Work .....	64
LIST OF REFERENCES.....		66
APPENDIX A.....		69
A.1	Basics of Labview Setup.....	69
A.2	Sensor Calibration Data.....	72
APPENDIX B .....		74
B.1	Convection Coefficient between the Air and Outer Wall.....	74
B.2	Convection Coefficient between the Water and the Inner wall .....	75
APPENDIX C .....		78
C.1	The Inference Error on the Temperature of Water from the Source of Error of the Sensor on the Outer Wall of the Pipe.....	78
C.2	The Inference Error due to the Source of Error of the Temperature of the Air .....	78

## LIST OF TABLES

<u>Table</u>	<u>page</u>
Table 4-1 Specifications of Cast-Acrylic Pipe.....	24
Table 4-2 Pipe Properties.....	36
Table 4-3 Physical Characteristics of Water at the Atmospheric Pressure.....	36
Table 5-1 Resistance of the Samples of the Randomly Distributed CNTs.....	41
Table 5-2 Tests on Sample 1.....	44
Table 5-3 Tests on Sample 2.....	46
Table 5-4 Performance of the CNT Films with Different Initial Resistance.....	47
Table 5-5 Samples Subject to Increasing and Decreasing Temperature Field .....	48
Table 5-6 Well-aligned CNT film Temperature Performance.....	49
Table 5-7 Temperature Dependence of the Deposited Films .....	55

## LIST OF FIGURES

<u>Figure</u>	<u>page</u>
Figure 1.1 The Concept of Sameness. Site 1 and Site 2 are where the signals are acquired. (a): the two signals are considered as being at the same site; (b) the two signals are considered as being not at the same site .....	3
Figure 2.1 Schematics of the Smart Wheel System.....	9
Figure 2.2 Structure of the FBG Sensor.....	10
Figure 2.3 Schematic of a Bi-functional Sensor Array.....	12
Figure 2.4 Temperature/pressure Sensor Concept.....	13
Figure 2.5 Possible Schematic of Pressure Measurement .....	14
Figure 2.6 Schematic of Temperature Transducer.....	15
Figure 3.1 Schematic of Signal Mapping .....	18
Figure 3.2 Correspondence between Sub-structures and Signals; (a) uncoupled; (b) coupled; (c) decoupled .....	19
Figure 4.2 Steady-state Temperature Distribution within a Plane Wall .....	26
Figure 4.3 Data Acquisition System .....	29
Figure 4.4 The Pipe and RTD.....	30
Figure 4.5 Electronics for Data Acquisition System .....	31
Figure 4.6 Typical 4-wire Resistance Measurement.....	32
Figure 4.7 Temperature Adjustable Circulator .....	33
Figure 4.8 Temperature Response of the RTD on the Outer Wall .....	35
Figure 5.1 Schematic of the tested CNT Film .....	40
Figure 5.2 Hotplate for Temperature Adjustment.....	41

Figure 5.3 Well-aligned CNT Film.....	42
Figure 5.4 Temperature and Resistance Measuring Process .....	43
Figure 5.5 Relationship between Temperature and Resistance (Sample 1).....	45
Figure 5.6 Relationship between Temperature and Resistance (Sample 2).....	46
Figure 5.7 Relation between Temperature and Resistance (Samples with Different Initial Resistance) .....	47
Figure 5.8 Film Performance Regarding Linearity and Hysteresis .....	49
Figure 5.9 Temperature Performance of the Well-aligned CNT Film.....	50
Figure 5.10 CNT Film Sample Prepared for Deposition .....	51
Figure 5.11 Polyaniline Solution Prepared for Electrochemical Deposition .....	52
Figure 5.12 Building of Electrochemical Cell .....	52
Figure 5.13 Prototypes for Temperature Measurement and pH Detection.....	53
Figure 5.14 Results after the Acid Doping .....	54
Figure 5.15 Test of Temperature Dependency of the CNT Film Deposited with Polyaniline .....	54
Figure 5.16 Resistance Change of Two PANI-modified Films .....	56
Figure 5.17 U-shaped Temperature Dependence.....	57
Figure 5.18 Temperature Dependence of Pristine and Oxidized CNT Composites.....	58
Figure 5.19 Temperature-dependent Resistivity of an Unintentionally Doped Bulk SWNT Film for Two Heating and Cooling Cycles .....	59

## LIST OF ABBREVIATIONS

<u>Abbreviation</u>	<u>page</u>
OSOS—One Sensor for One Signal .....	1
SSST—Acquiring Multi-Signal at the Same Site and Same Time.....	1
OSMS—One sensor for Multi-signals.....	1
SWNTs—Single Wall Carbon Nanotubes.....	13
VANTAs—Vertically-Aligned Nanotube Arrays .....	13
DFM—Design for Modeling .....	18
FR—Functional Requirement.....	22
CR—Constraint Requirement.....	22
DP—Design Parameter .....	24
PP—Process Parameter.....	25
PANI—Polyaniline .....	50
PMMA—Methylmethacrylate .....	40
MWNTs—Multi-Walled Carbon Nanotubes.....	40
DMSO—Dimethyl Sulfoxide .....	51
VRH—Variable-range Hopping .....	56
PVDF—Polyvinylidene Fluoride.....	57

## CHAPTER 1 INTRODUCTION

CHAPTER 1 includes five sections—motivation, research problem, research objectives and scope, overview of methodology, and thesis organization.

### **1.1 Motivation**

Since the last decade, sensor technology has advanced rapidly due to the development of internet-based technology and nano-technology. This rapid advancement has been motivated by increased application usage of sensor technology in many areas, including military applications, infrastructure surveillance, medical operations, and civil communication applications [1]. There are two characteristics with the contemporary applications of sensors: (1) network deployment to cover a large area and (2) acquisition of multi-signals at the same site [2, 3].

The current sensor technology is primarily comprised of *one sensor for one signal* (OSOS). This unfortunately cannot satisfy the applications with the above-mentioned characteristics due to various problems. There is increasing demand to have smaller target systems. This is a problem because the density of the sensor may be too high for that particular sized target system. Another problem with the OSOS is the difficulty in ensuring that two or more signals are actually coming from one location or site at the same time. Therefore, it is of interest to have a sensor that acquires multi-signals at both *the same site and the same time* (SSST).

Research presented in this thesis aims to address the aforementioned problems with the OSOS. In particular, this research aims to develop a new paradigm of sensor technology whereby one sensor can acquire multi-signals at the same place and at the same time. This new paradigm is, in short, called *one sensor for multi-signal* (OSMS). Research in this thesis was limited to one sensor for two signals as an example in an attempt to demonstrate the multi-signal acquisition theory.

## 1.2 Research Problem

Prior to defining the problem motivating this research, it is necessary to clarify concepts related to OSMS. A signal is an entity that gives information in a particular context. For example, consider the entity that represents the pressure of a blood vessel/artery in the auscultatory method [4], in which systolic blood pressure is read when the first sound of beep occurs after the cuff pressure is released and diastolic pressure is read until no sound can be heard. In this thesis, blood pressure would be referred to as the stem signal and systolic and diastolic pressure would be referred to as end signals. The relation of the stem signal and the end signal is of relativity. Signal A may be an end signal in respect to signal B, but it may be viewed as a stem signal in respect to signal C. In this thesis a signal refers to the end signal in a particular context, and thus represent a particular piece of information.

Another concept that needs to be clarified is related to SSST. Sameness of location or site also follows the relativity principle. This means that any site that physically occupies a space (see Figure 1.1) and the information from any place within this space is considered the same. Let us denote this space by  $A_p$ . The probe to sense information from a site also occupies the space. That

is, the probed information in this space is considered the same. Let us denote the space covered by the probe as  $A_p$ . The notion of sameness in terms of site is thus only valid when  $A_p \geq A_s$ .

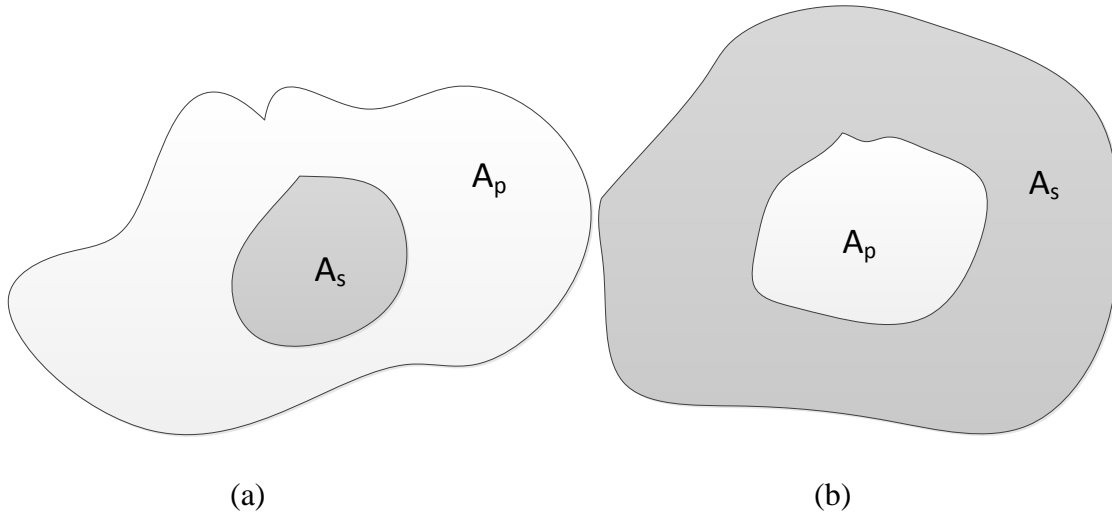


Figure 1.1 The Concept of Sameness. Site 1 and Site 2 are where the signals are acquired. (a): the two signals are considered as being at the same site; (b) the two signals are considered as being not at the same site

The above discussion regarding the notion of sameness in terms of space or site is also applicable to the notion of sameness in terms of time. This means that there should be  $t_p$  that denotes the time interval in which information is considered to be the same.  $t_s$  which denotes the time interval in which a probe picks the two signals. Likewise, the sameness in terms of time makes sense only when  $t_p \geq t_s$ .

On a general note, the nature of the relativity in this thesis is that, given an entity or a system, its behavior governed by its intrinsic principle may differ from that perceived by an observer who is outside the system.

The main research problem is therefore to develop a sensor that acquires two signals by satisfying the condition of  $A_p \geq A_s$  and the condition of  $t_p \geq t_s$ . Ideally, the smaller the area  $A_p$  is

and the smaller the time interval  $t_p$  is, the more sense of sameness can be achieved. This further implies that the smaller  $A_s$  and the smaller  $t_s$ , the better performance of a OSMS sensor. The main challenge for developing OSMS technology is thus to reduce  $A_s$  and  $t_s$ ,

### **1.3 Research Objectives and Scope**

The nature of this thesis research is to advance our understanding of multi-signal sensing and develop technology for multi-signal sensors. Two objectives are defined for this thesis to conduct research to prove this hypothesis:

**Objective 1:** Investigate the governing principle of an OSMS sensor. The governing principle refers to the knowledge of how an OSMS sensor acquires two signals at the same site and same time. Such a principle can also be viewed as the transducer principle of the OSMS sensor.

**Objective 2:** Develop demonstration prototypes that can be used to prove that the principles proposed from Objective 1 are valid. Signals in this study were focused on pressure, temperature, and the pH value.

This research is restricted to concept development. Multi-signals in this thesis refer to two signals only without loss of generality.

### **1.4 Overview of Methodology**

The proposed research is a pilot study of the new sensor paradigm OSMS. It explores the working principle that governs the OSMS sensor and provides case studies to assess the feasibility of OSMS sensors. In designing and building the case system, the general design

theory and methodology such as systematic design procedure was employed. That systematic design procedure puts emphasis on the rigorous formation of the design problem defined by the functional requirement and constraint requirement [5]. Then, the design is to find solutions to meet requirements. Another design theory and methodology is called Axiomatic Design Theory (ADT) [5]. This theory consists of two axioms for achieving a best design. The first axiom says that the best design is the one, which can maintain the function independency, and the second axiom says that best design is the one chosen from the design options (that all meet the first axiom) with minimal information content. Further, in ADT, there is a notion called uncoupled design, decoupled design and coupled design [5], and this notion is employed to derive the working principle for OSMS sensors.

## **1.5 The Organization of the Thesis**

The thesis consists of six chapters and they are organized as follows.

Chapter 1 provides background information to clarify the motivation for this research, research problems and associated challenges, general research hypotheses and objectives, and finally a listing of the methodologies used in this research. The first section of this chapter paints a background and prompts the motivation for this research. The second section derives the research problems and their challenges. The third section gives the general research hypothesis and objectives. The fourth section outlines the general research methodology used by this thesis.

Chapter 2 provides a comprehensive literature review and further background information. This includes a discussion of the nature of the research, justification of novelty, and the originality of the work described in this thesis.

Chapter 3 further discusses the concept of multi-signal acquisition sensors and proposes several general principles for designing such a sensor.

Chapter 4 and Chapter 5 provide two case studies to demonstrate how the proposed principles can be practically used in OSMS applications.

Chapter 6 gives an overview of the work performed in this research, draws conclusions, and justifies the contributions of this thesis. A future direction of work is also outlined in this chapter.

## CHAPTER 2 LITERATURE REVIEW

Section 2.1 will provide a general review of sensors. Section 2.2 will review several important sensor studies with their achievements relevant to OSMS. Section 2.3 provides concluding remarks.

### **2.1 Preliminary Concept**

A sensor is a device that measures signals at a site ( $s$ ) at a time ( $t$ ). The nature of a sensor is to represent a meaning, signal, or information by means of a quantity that has a clear magnitude. This quantity often refers to an electric quantity such as charge, current, resistance, etc., as this type of quantity has magnitude. When the electric quantity is linearly proportional to the signal to be measured, the quantity becomes a surrogate of the signal. The signal is tied to the surrogate with a constant coefficient.

There are two remarks about the nature of sensors. Remark 1: the relationship between the surrogate and the signal may not necessarily be linear. Non-linearity can produce a huge difficulty in actual use of such a sensor. For this reason, only surrogates that have a linear relationship with a signal is sought for the field of sensor technology. Remark 2: the surrogate may not necessarily be an electric signal but it can be any measurable signal, e.g., color.

The transfer device between the surrogate and the signal is called a transducer. It is noted that when an electric surrogate is imposed on a transducer to produce movement, the transducer is also called an actuator. Therefore, a sensor and an actuator represent two opposite functions of a transducer.

The notion of “one” site and “one” time is from the notion of relativity. The “one” here depends on the application problem. For instance, a complete building may be considered as “one” place or site when it is seen from an airplane. However an observer who is inside the building will not view the building as “one” site, but as a space with many different sites. The same concept is applied to the notion of “one” time as noted in Chapter 1.

## **2.2 Sensor Technology Developments Related to OSMS**

There are a few studies reported in literature, which have proposed methods similar to OSMS (none of them have however coined the word “OSMS”). In the following section, these studies are reviewed and analyzed to show the state-of-the-art OSMS technology.

### **2.2.1 The Work of Lin’s Group**

Lin’s Group at Northeastern University (USA) is, perhaps, the first group to explore OSMS [6, 7]. They attempted to develop an OSMS on the steering wheel (see Figure 2.1) in a vehicle to acquire multiple physiological signals of the driver during driving. The signals include body temperature, pulse wave, and blood alcohol level.

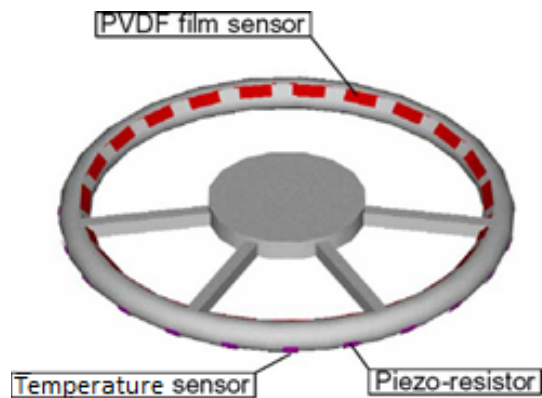


Figure 2.1 Schematics of the Smart Wheel System [7]

The principle of their OSMS is that three transducers are in place for three signals. The transducers were forged on the wheel in a predetermined pattern. Their latest work was to apply nanotechnology to make two of the transducers extremely small in order to measure temperature and pressure [8]. The principle of OSMS in Lin’s Group developments is to put multiple transducers side-by-side. However, the system developed by this group has an inherent limitation regarding the one site concept proposed in this thesis, as the “same site” referred in their work is limited by the size of the transducer, i.e., the space that side-by-side transducers occupy ( $A_s$ ) is more likely to exceed the information space ( $A_p$ ).

### 2.2.2 Fiber Bragg Grating Sensor for Temperature and Strain Measurement

Fiber Bragg Grating (FBG) is an effect that describes a linear relation between the wavelength of incident light and the grating engraved on the fiber. This effect has been explored to allow measurement of both temperature and pressure signals from a target system where a FBG is embedded or placed [9-11].

Figure 2.2 shows a schematic diagram of the sensing principle [12] for measuring strain and temperature simultaneously. The measurement system has two grating fibers that are exposed under one UV light. They are fabricated with different refractive indexes into different FBGs. The two FBGs have a spliced joint. Further, Fiber 2 is attached with an aluminum substrate flake, which results in a significantly different thermal expansion of fiber 2 from that of fiber 1. Therefore, fiber 2 is relatively more sensitive to temperature in comparison with fiber 1. The bounding also makes the straining effect on fiber 2 much less than that on fiber 1.

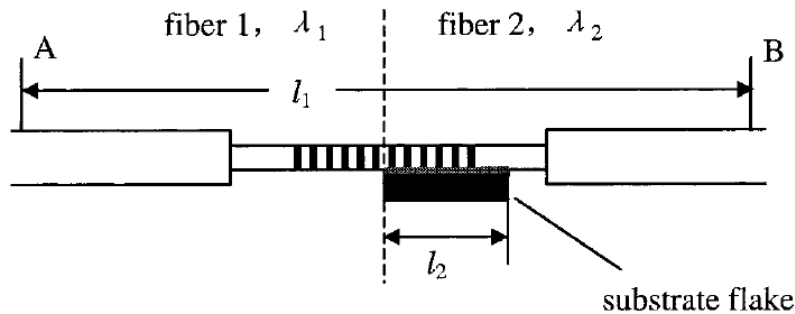


Figure 2.2 Structure of the FBG Sensor [12]

One can adjust the incident light so that the FBG phenomenon occurs. One can see two peaks corresponding to the FBGs using an optical scope. The relation between the incident light and the coefficient of the FBG is known. Therefore, by prescribing the attribute of the incident light to induce the Bragg phenomenon one can then determine the coefficient in the FBG to obtain the information of temperature and strain with fiber 1 and fiber 2. It is noted that the relation of the coefficient of FBG with respect to temperature or pressure was known to the study.

The FBG approach, however, suffers from the limitation of the fiber size in terms of one site. This means that the sense of “one site” is restricted by the size of the fiber. If the size of “one site”

is less than the FBG sensor measurable range, the signals acquired in this case are thus not from the same site. This is because the nature of the FBG approach to acquire multiple signals is a side-by-side arrangement of multiple transducers.

### 2.2.3 Magneto-Elastic Micro-Sensor Array

Magneto-elastic sensor is characterized as a resonant frequency-emitting device. The resonant frequency of the sensor is a linear function of elastic modulus, Poisson's Ratio, density, and length. These properties may change in response to multiple ambient factors such as temperature, pressure, flow rating, mass loading, and so on.

The basic working principle of the Magneto-elastic sensor is as follows [13]. Put the magneto-elastic material under the field of a signal to be measured (e.g., temperature) while at the same time the material is subject to a physical stimuli which has frequency (i.e., magnetic flux in this case). By adjusting the stimuli's frequency to the extent that the material is under the resonant state, the resonant frequency is obtained. Then, the respective property of the material can be found based on property-resonant frequency relation. Subsequently, the signal is found from the property-signal relation.

For multiple signals acquisition, first transducers for these signals are arranged side-by-side, and then a structure that decouples the multiple signals is designed. The OSMS in this case is composed of these transducers and decoupling structure.

The OSMS sensor, based on above working principle (i.e., the Magneto-elastic material), has been reported in literature [14] in which temperature and pressure are simultaneously measured.

However, the limitation of such OSMO sensors is the same as FBG; that is, the accuracy of the sensor, in terms of one site, is dependent on the size of the transducers and decoupling structure.

#### 2.2.4 Thin Film Technology for Multi-signal Acquisition

Figure 2.3 is a design of a flexible composite foil polymeric ferroelectric matrix embedded with ceramic ferroelectric nanoparticles [15]. In (a), the piezoelectric elements have an opposite parallel-orientation of the polarization of the ceramic particles, while the pyroelectric elements have a parallel-orientation of the polarization of the ceramic particles. In (b), it shows an equivalent electrical circuit of the sensors. In (c), a prototype of the sensor is shown.

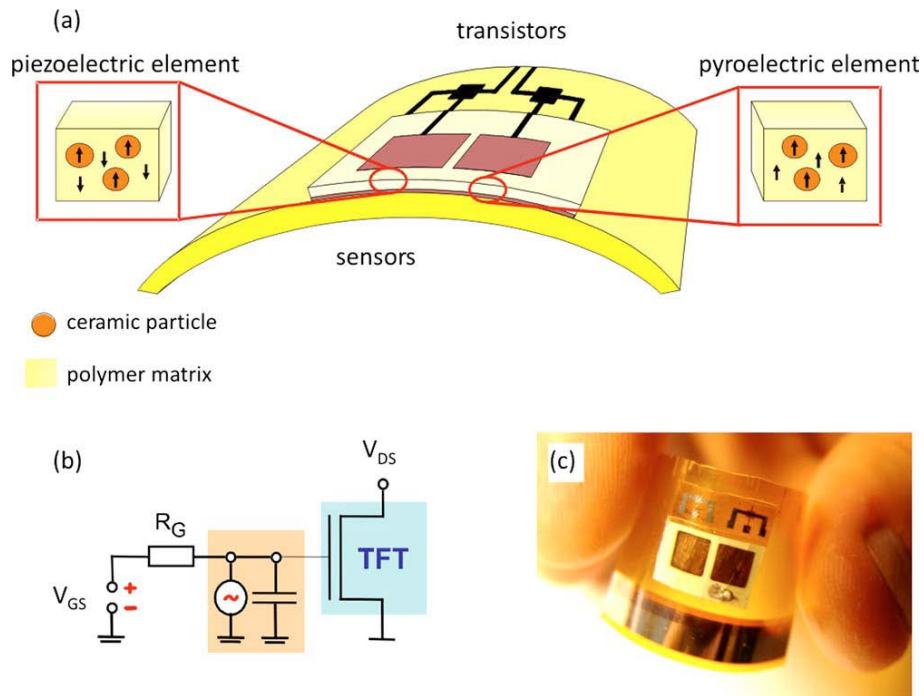


Figure 2.3 Schematic of a Bi-functional Sensor Array [15]

This device features a unique structure that enables the two opposite effects to exhibit at the same time with two stimuli. In particular, the pyroelectric composite works as a temperature sensitive unit while the piezoelectric composite works as a pressure sensitive unit.

The benefit of this device is due to the decoupling mechanism of nanoparticle polarization with respect to the temperature and pressure stimuli. In regards to the measured object, the status of the parameters is currently unknown. From Figure 2.3 it is clear that the two electrodes are aligned in such a way that temperature and pressure may not come from the same object. To generalize the concept of multi-signal, this research group has yet to derive a fundamental underlying theory.

The latest invention based on carbon nanotubes has created a concept that temperature and pressure could be measured simultaneously without having a significant coupling issue [16]. As it can be seen from Figure 2.4, the transducer is a polymer matrix that contains two different groups of carbon nanotube structures, including a temperature transducer and a pressure transducer. The temperature measurement is derived from the thermal couple arrangement of Single Wall Carbon Nanotubes (SWNTs). The pressure measurement is derived from the substrate that is fixed with the Vertically-Aligned Nanotube Arrays (VANTAs). A specific decoupling mechanism for pressure measurement and temperature measurement is employed by having a proper design of the configurations of these two groups of carbon nanotubes.

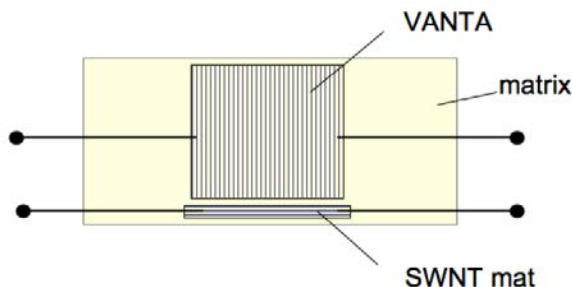


Figure 2.4 Temperature/pressure Sensor Concept [16]

The pressure measurement comprises a plurality of VANTA, which are under compression along the axial direction, inducing bends and twists among the tubes (see Figure 2.5). Thus, the junctions between the tubes spontaneously increase and cause the resistivity loss between the electrodes. The resistivity change was proved to be linear within a certain range [16].

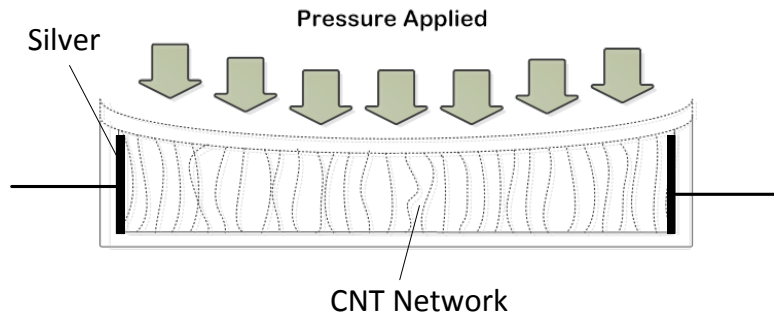


Figure 2.5 Possible Schematic of Pressure Measurement

The temperature measurement is achieved by configuration of the thermocouple, where two single tubes with similar properties connect to each other at one end creating only one junction (Figure 2.6). The junction resistivity appears to have a linear change caused by temperature variations. By controlling the number of junctions, Ivanov et al. have successfully isolated the temperature influence over the pressure measurement [16]. However, whether or not the pressure measurement is subject to temperature change is unknown.

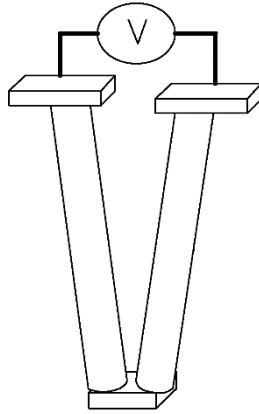


Figure 2.6 Schematic of Temperature Transducer [16]

### 2.3 Concluding Remarks

There are various proposed approaches in the literature for acquiring multiple signals. However, most approaches and principles are side-by-side arrangements of multiple transducers, including the FBG sensing principle and Magneto-elastic sensing principle. There has been much effort on integrating multiple transducers instead of the side-by-side arrangement, namely the work by Ivanov et al. [17]. However, there are no theories available for OSMS technology.

## CHAPTER 3 PRINCIPLES FOR MULTI-SIGNAL ACQUISITION

This chapter presents the governing principle for the OSMS. The governing principle here refers to the sensing principle. Note that in this thesis, sensing is not just about the transducer but also about transducer plus the means of exhibiting the signal or information (see Section 2.1). Therefore, a sensing principle describes a pathway or mechanism from a change in physical attribute to a change in the form of signal with a sensing device. Further, the sensing principle here, in particular, refers to the principle that allows for acquiring two signals with one sensor, namely the principle of OSMS, rather than the transducer principle for acquiring one signal with one sensor in the traditional sensor technology. At this point, three principles of OSMS are proposed and presented in this chapter.

### **3.1 Principle 1: Acquiring Multiple Signals through a Stem Signal**

Principle 1 proposes that two signals are obtained with different signal acquisition methods from the same stem signal. One example of the OSMS sensor that follows this principle refers to the sensor that measures the amount of  $H_2S$  and checks the presence of hemoglobin. This sensor was previously developed by our group [17].

The sensor body was a cluster of pristine carbon nanotubes (p-CNTs). The target system was a fluid that contained  $H_2S$  and hemoglobin chemicals. This sensing has the following steps [17]:

- Step 1: a p-CNT probe was immersed in the target system for about 5 minutes.

- Step 2: the p-CNT probe was examined by Raman Spectroscopy and Raman Microscopy.
- Step 3: the presence of hemoglobin in the target system was checked with wave-number shift in the Raman Spectrum [18].
- Step 4: the amount of H<sub>2</sub>S was calculated from the relation between the intensity of the Raman Luminescence response to sulfide element attached on the p-CNT and the amount of sulfide element [19].

The measurement of blood pressure in artery is another example of the OSMS sensor based on Principle 1. However, the two signals (systolic pressure and diastolic pressure) are obtained at different time points. In contemporary medical applications this time interval is widely accepted, this is why the measurement of blood pressure by the method of systolic pressure and diastolic pressure falls into the category of OSMS.

### 3.2 Principle 2: One Signal Inference and One Signal Measurement

This principle proposes an OSMS sensor that has only one signal (A) that can be accurately and efficiently inferred by the corresponding transducers in the neighboring sites (S<sub>1</sub>, S<sub>2</sub>, S<sub>3</sub>...). Figure 3.1 shows a schematic diagram of this principle. At site A, the signal is required to be measured. The sensor for X is not directly placed at site A, but it is placed at 1, 2, 3..., n (n represents the total number of sensors for X). The signals at 1, 2, 3 ..., n are mapped to the signal at site A by

$$S_A = F_A(S_1, S_2, S_3, \dots, S_n) \quad (3.1)$$

where  $S_1, S_2, S_3, \dots, S_n$  are signals at Site 1, 2, 3 ..., n.  $F_A$  is a mapping function from  $S_1, S_2, S_3, \dots, S_n$  to  $S_A$  and  $S_A$  is the signal at Site A.

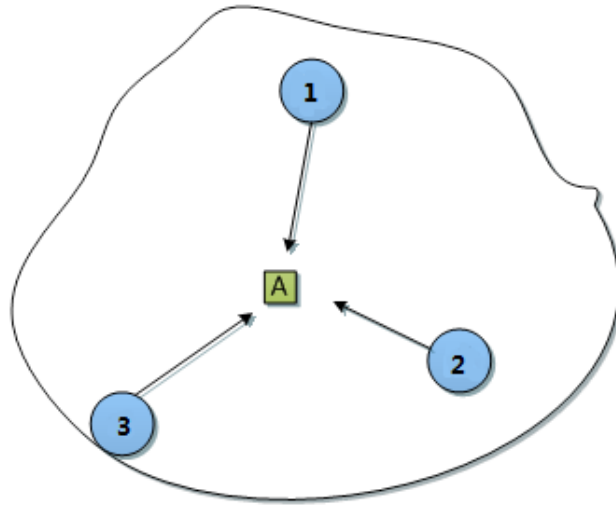


Figure 3.1 Schematic of Signal Mapping

With this principle the accuracy of sensing is dependent on the accuracy of the mapping function  $F_A$ . Therefore, the structure of the OSMS, which contains Site 1, 2, 3..., n and A, must be designed to render an accurate  $F_A$ . This design philosophy is called “Design for Modeling” (DFM). DFM can be generalized as the design of the structure such that the mathematical model of a behavioral state of the structure can be very accurate.

### 3.3 Principle 3: Acquiring Multiple Signals through a Multi-transducer Structure

This principle proposes building a composite material with multiple transducers. At first, the notions of uncoupling and decoupling will be elaborated, and then a discussion will be presented regarding the principle.

A sensor body is viewed as a system, so it has a structure. The structure can be decomposed into sub-structures. These sub-structures are described by parameters ( $P_1, P_2, \dots, P_n$ ). Each sub-

structure corresponds to one signal: the correspondence between the sub-structures and signals are noted, and there are three possibilities.

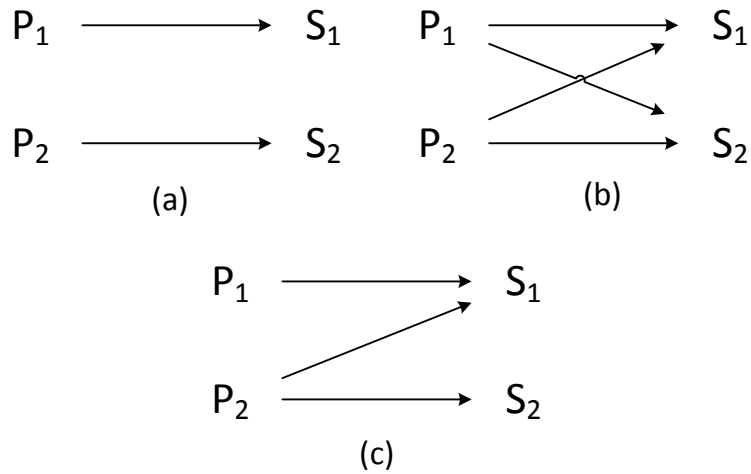


Figure 3.2 Correspondence between Sub-structures and Signals; (a) uncoupled; (b) coupled; (c) decoupled

In the design literature [20], the three cases are called (a) uncoupled, (b) coupled, and (c) decoupled. Among the three, the decoupled relationship needs further explanation. Decoupling means that through a proper order of sensing, a coupled case can be made as if it were uncoupled. For example, in Figure 3.2(c), a change in P<sub>1</sub> is an indication of S<sub>1</sub>, but a change in P<sub>2</sub> is a joint indication of S<sub>1</sub> and S<sub>2</sub> (i.e., a change in P<sub>2</sub> could be contributed by both S<sub>1</sub> and S<sub>2</sub>). If the order of sensing can be changed such that (1) reading P<sub>1</sub> for S<sub>1</sub>; (2) reading P<sub>2</sub> for a combined S<sub>1</sub> and S<sub>2</sub>; (3) getting S<sub>2</sub> from P<sub>2</sub>-P<sub>2</sub>(S<sub>1</sub>) where P<sub>2</sub>(S<sub>1</sub>) is the part of P<sub>2</sub> contributed by S<sub>1</sub>. Consequently, S<sub>1</sub> and S<sub>2</sub> are made uncoupled. Therefore, the structure of OSMS by following Principle 3 will have either an uncoupled structure or a decoupled structure.

There are two remarks on these principles for the OSMS sensor and they are discussed as follows:

Remark 1—these three principles can co-exist on one OSMS sensor; Remark 2—an OSMS sensor with two side-by-side transducers is a special case of Principle 3. However, the accuracy

of this type of OSMS sensors is limited due to the challenge related to the Area of ( $A_S$ ) (in Figure 3.1). Chapter 4 and Chapter 5 will present two case studies for Principle 2 and 3 only, because Principle 1 appears well-proven, e.g., blood pressure measurement case as mentioned in Chapter 1.

## CHAPTER 4

### CASE STUDY I: PROOF OF PRINCIPLE 2 FOR OSMS

In this chapter, a case study to prove Principle 2 for OSMS is presented. The challenge involves measuring temperature and pressure at one place simultaneously. In particular, the target system is a pipe in which a fluid with a certain temperature flows through it. The pipe system is required to simultaneously obtain the information of both the temperature and pressure from one place on the inner wall of the pipe. This chapter is organized as follows: Section 4.1 gives details about the target system and in particular about its functional requirement as well as its constraint requirement. Section 4.2 presents the design of the OSMS sensor by following Principle 2, as discussed in Chapter 3. Section 4.3 describes the experiment setup for measuring the temperature on the inner wall. Section 4.4 presents the results and an accompanying discussion. Section 4.5 provides conclusions .

#### **4.1 A Pipe System for Temperature and Pressure Measurement**

The objective of this study was to measure temperature and pressure on the inner wall of a pipe at the same site and same time. A sensor to measure pressure was supposed to be placed on the inner wall; however, it was difficult to put another sensor in the same location in order to measure temperature. This difficulty may be because the sensor cannot be subjected to the high temperature of the fluid in the pipe. This resulted in the sensor for temperature being placed on the outer wall of the pipe, but inferring the temperature on the inner wall. Therefore, Principle 2 for OSMS can be applied in the development of this OSMS sensor (for pressure and

temperature), in particular by having a model that can infer the temperature on the inner wall of the pipe from the temperature on the outer wall of the pipe. Note that there is a sensor to measure the temperature on the outer wall of the pipe.

Figure 4.1 shows a schematic diagram of the pipe with sensors for temperature measurement. According to Principle 2, the design of the pipe system should follow this strategy: (1) to design a pipe system that fulfills its own primary function (**FR**: functional requirement), while the function may further be subject to some constraint (**CR**: constraint requirement); (2) to modify the system resulting from (1) to facilitate building an accurate model for signal inference.

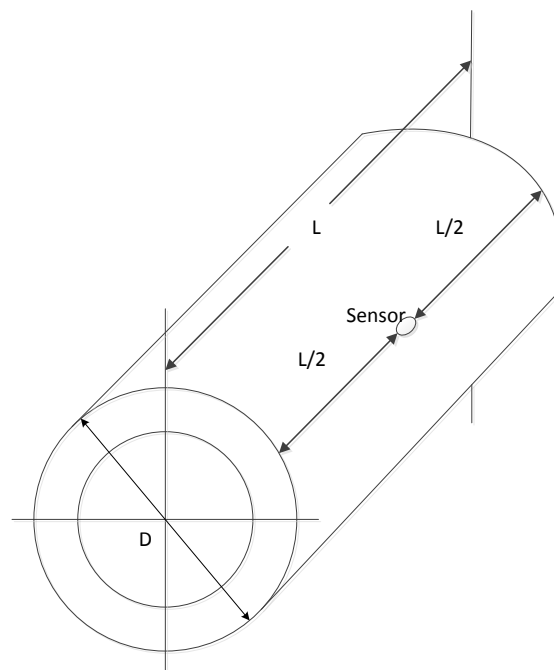


Figure 4.1 Schematic of the Pipe System

The Functional Requirement (FR) of the pipe is that the pipe contains a fluid with a stable axial velocity running inside. The constraint requirement (CR) of the pipe includes:

- a. There should not be any pressure leakage at the pipe connector. **CR-1**.

- b. The fluid system must reach steady-state as soon as possible when the flow starts. **CR-2.**
- c. The fluid inside the pipe must be fully developed. **CR-3.**
- d. The fluid inside the pipe should be single phase. **CR-4.**

Further, there are constraints related to Design For Modeling (DFM) that are associated with Principle 2. DFM is a design principle that states that a system under design for functionality should be constructed in such a way that the assumptions behind the model of the system's behavior are as correct as possible.

Based on the DFM, several constraints were further proposed called DFM constraint (DFM-C).

They are described below:

- a. The temperature sensor should be placed somewhere near the middle point of the pipe along its longitudinal axial direction because this point seems to be most insensitive to disturbance (in comparison with other points along the axial direction of the pipe). **DFM-C-1.**
- b. The material of the pipe should have a relatively low thermal conductivity, ideally lower than  $0.5 \text{ W}/(\text{m}\cdot\text{K})$ , and it should have very low radiation heat transfer. **DFM-C-2.**
- c. The pipe does not have any significant alteration under the testing conditions. **DFM-C-3.**
- d. The pipe must maintain its horizontal position during the tests. **DFM-C-4.**
- e. There should be no significant turbulence in the room and the room temperature should remain stable. **DFM-C-5.**

The design parameter (**DP**) was then determined based on the FR, CR, and DFM-C. The DP is presented as follows:

- a. One temperature sensor is put on the outer wall. The sensor has a rectangular shape with the specification of 1.25×1.7mm (small enough to attach it on the outer wall), a thermal response of 0.1s, and a temperature range of -50°C to +500°C. **DP-1** (satisfying DFM-C-1).
- b. The pipe specification is shown in Table 4-1. In particular, the material was a cast-acrylic paper that is transparent (so radiation heat transfer is very small). **DP-2** (satisfying DFM-C-2 as well as satisfying CR-1).
- c. The pipe is horizontally laid down. **DP-3** (Satisfying CR-2 as well as satisfying DFM-C-4).
- d. The pipe is put in the room environment. **DP-4** (Satisfying DFM-C-3, DFM-C-5).

Table 4-1 Specifications of Cast-Acrylic Pipe

Properties	Values
Thermal Continuous Service Temperature in Air	85°C
Heat Deflection Temperature	110°C @66 PSI, 133°C @264 PSI
Coefficient of Linear Expansion	6.1×E-5 cm/cm/°C
Thermal Conductivity	0.2W/(m·K)
Specific Heat	1470 J/(kg·K)
Pipe Sizes	O.D. 63.23 mm, I.D. 50.90 mm, 317 mm in length

Since the pipe system is a process system, the process parameters (**PP**) also contribute to the function of the system as well as the constraints that the system is subject to. The **PPs** were determined as follows:

- a. The environment where the pipe stays had a central temperature control system that can maintain a constant temperature and an air stream system that produces the condition for a natural convection to take place between the pipe and the air. **PP-1** (satisfying DFM-C-3).
- b. The fluid running was kept (in order to reach a steady state of the fluid). **PP-2** (satisfying CR-3, CR-4).

## 4.2 Temperature Inference Model Development

The model was based on the following assumptions:

Assumption 1: radiation heat transfer is negligible.

Assumption 2: only one dimension heat transfer , i.e., the radial direction.

Assumption 3: The factors such as density variation, viscous dissipation, and edge effects, which compromise the continuous fluid, are considered negligible.

Assumption 4: The flow is steady-state.

Figure 4.2 shows a path of heat transfer across the pipe. It is noted that the general equation for the convection heat transfer is as follows (see Figure 4.2):

$$q_c = \bar{h}_c A (T_1 - T_\infty) = \frac{(T_1 - T_\infty)}{1 / \bar{h}_c A} \quad (4-1)$$

where  $\bar{h}_c$  is the convection coefficient,  $A$  is the conduction surface area,  $1/\bar{h}_c A$  is the convective resistance, and  $q_c$  is the heat flux. The heat transfer from the side of the inner wall of the pipe to the side of the outer wall of the paper can be expressed by:

$$\bar{q}_r = \frac{T_{\infty 1} - T_{\infty 2}}{\frac{1}{\bar{h}_{c1}A} + \frac{L}{KA} + \frac{1}{\bar{h}_{c2}A}} \quad (4-2)$$

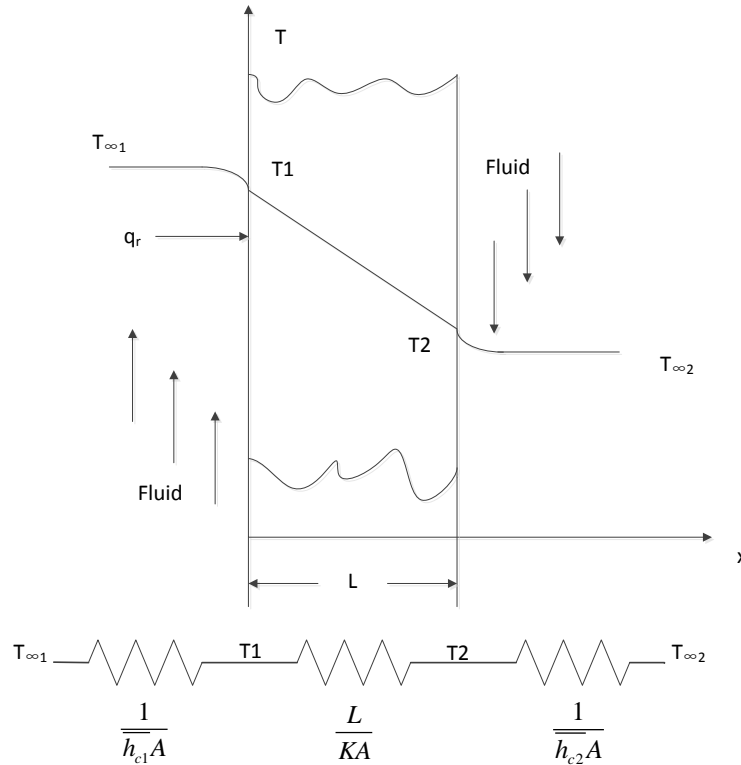


Figure 4.2 Steady-state Temperature Distribution within a Plane Wall

where  $K$  is the conductivity coefficient of the wall. Equation (4-2) [21] can be further written as

$$\bar{q}_r = \frac{T_{\infty 1} - T_{\infty 2}}{R_{c1} + R_k + R_{c2}} \quad (4-3)$$

where  $R_{c1} = \frac{1}{\bar{h}_{c1}A_1} = \frac{1}{\bar{h}_{c2}2\pi R_1 L}$ ,  $R_k = \frac{\ln(R_2/R_1)}{2\pi kL}$ ,  $R_{c2} = \frac{1}{\bar{h}_{c2}A_2} = \frac{1}{\bar{h}_{c2}2\pi R_2 L}$ .

$$\bar{q}_r = \frac{T_{\infty 1} - T_{\infty 2}}{R_{c1} + R_k + R_{c2}} = \frac{T_{\infty 1} - T_1}{R_{c1}} = \frac{T_1 - T_2}{R_k} = \frac{T_2 - T_{\infty 2}}{R_{c2}} \quad (4-4)$$

From Equation (4-4), the water temperature can be derived. First, from Equation (4-4), the following relations can be obtained.

$$\begin{cases} T_1 = \bar{q}_r R_k + T_2 \\ T_1 = T_{\infty 1} - \bar{q}_r R_{c1} \\ T_{\infty 1} - T_2 = \bar{q}_r (R_k + R_{c1}) \end{cases} \quad (4-5)$$

From Equation (4-5), the following equation yields:

$$T_{\infty 1} = T_2 + \bar{q}_r (R_k + R_{c1}) \quad (4-6)$$

It is noted that (see Figure 4.2) in the circumstance of the present case,  $T_{water} = T_{\infty 1}$ ,  $T_{out} = T_2$  where  $T_{out}$  represents the temperature on the outer wall of the pipe and  $T_1 = T_{in}$  represents the temperature on the inner wall of the pipe. Given these notations, Equation (4-6) is rewritten to

$$\begin{aligned} T_{water} &= T_{out} + \bar{q}_r (R_k + R_{c1}) \\ T_{water} &= T_{out} + \bar{q}_r \left( \frac{\ln \frac{D}{d}}{2\pi K} + \frac{1}{h_1 \pi D} \right) \end{aligned} \quad (4-7)$$

In Equation (4-7),  $D$  and  $d$  are the outer diameter and inner diameter of the pipe, respectively;  $K$  is the heat conductivity of the pipe; and  $h_1$  is the heat convection coefficient between the water and inner wall of the pipe.

Further, there is a convection heat transfer between the air and outer wall of the pipe, which is governed by

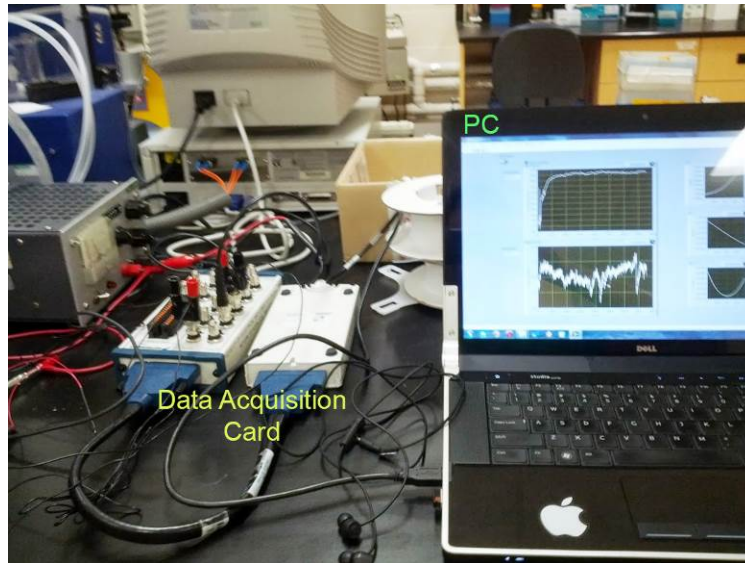
$$\bar{q}_r = \bar{h}_c D (T_{air} - T_{out}) \quad (4-8)$$

where  $\bar{h}_c$  is the convection coefficient between the air and the outer wall of the pipe.

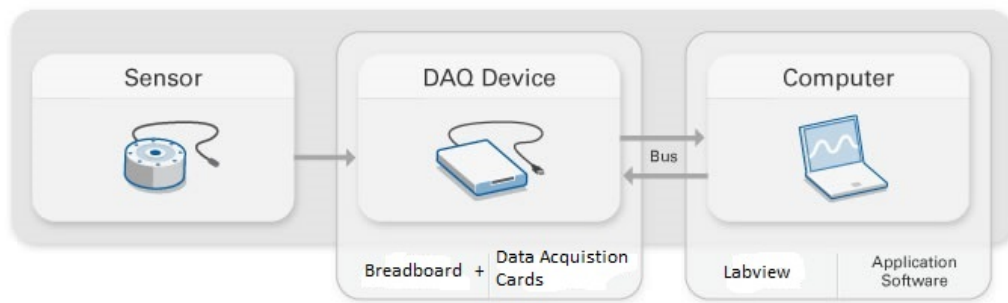
### **4.3 Experiment Setup**

#### **4.3.1 Data Acquisition System**

The data acquisition system is shown in Figure 4.3, and it primarily includes a data acquisition card, an analog-to-digital converter, a USB cable, and a laptop. The Labview program from National Instruments (Ver. 2012) was installed for the signal processing and analysis. Two channels of the data acquisition card were connected with two RTDs (PT1000) sensors, one of which was attached on the outer wall of the pipe; the other was set up to monitor the ambient temperature. The RTD can measure a temperature ranging from  $-50^{\circ}\text{C}$  to  $+500^{\circ}\text{C}$  with a nominal resistance of  $385\Omega$  (Between  $0^{\circ}\text{C}$  and  $100^{\circ}\text{C}$ ) (Figure 4.4). The Labview program was built upon a voltage collecting DAQ module plus low-pass filters, indicators, timers, graphs, and calculators. Details of the Labview configurations are presented in Appendix A.

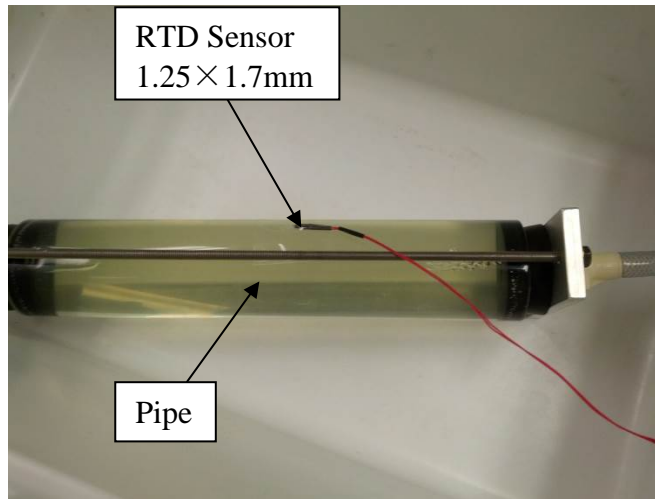


(a) Experiment Setup

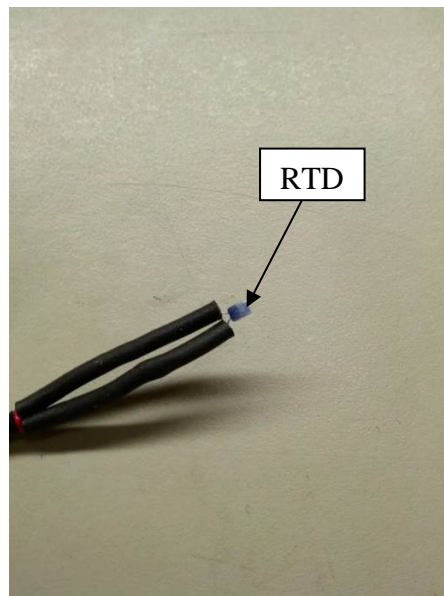


(b) Schematic Design

Figure 4.3 Data Acquisition System



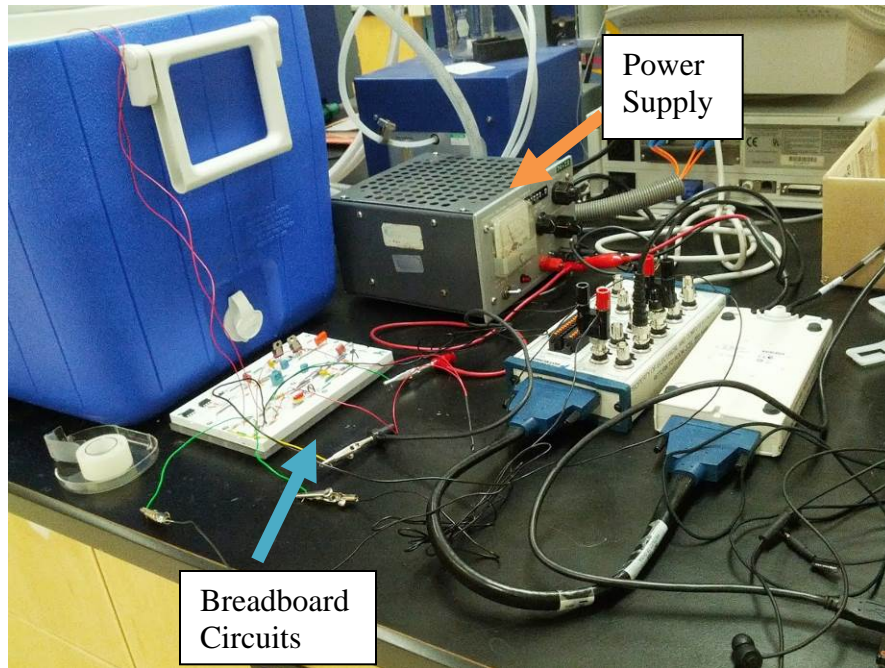
(a)



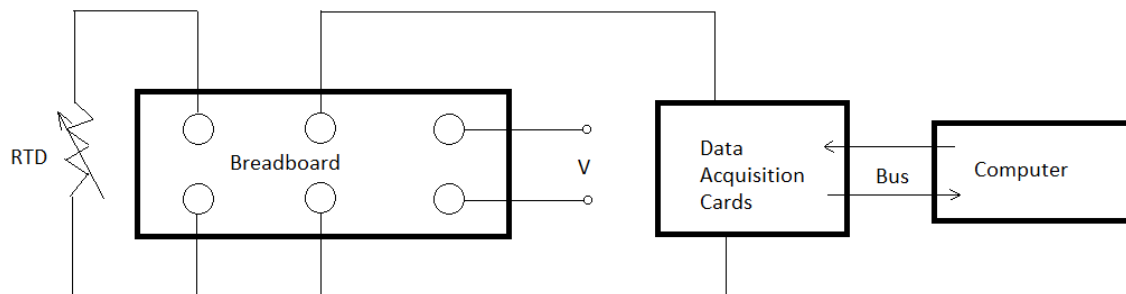
(b)

Figure 4.4 The Pipe and RTD

The RTD sensor was a PT1000 Class B model that measures  $1000\Omega$  at  $0^{\circ}\text{C}$  (its measurement error is about 0.3%). The sensor has a constant power supply that is configured through a breadboard (Figure 4.5).



(a) Experiment Setup



(b) Schematics of Data Acquisition System

Figure 4.5 Electronics for Data Acquisition System

The RTDs were connected through a typical 4-wire resistance measurement circuit (Figure 4.6) to increase measurement accuracy [22]. Because the constant current could not be digitally read from the power supply, the voltage was consequently substituted for the temperature calculations.  $R_1$ ,  $R_2$ ,  $R_3$ , and  $R_4$  are four stands of  $1\text{ K}\Omega$  resistors that are used to cancel the influence due to the resistance of the electrical wire (notice: the resistors are much greater than the wire), and

$R_T$  represents the resistance of the RTD. The Labview program automatically calculated the temperature output.

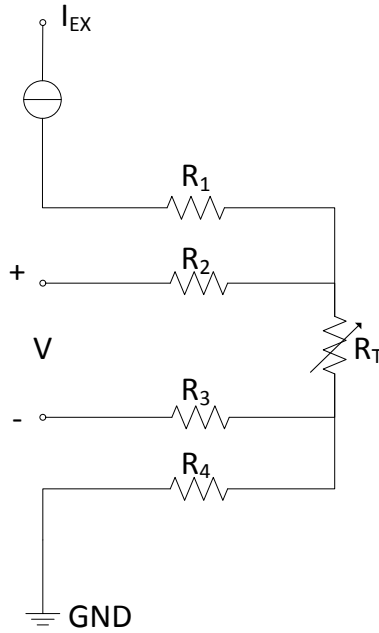


Figure 4.6 Typical 4-wire Resistance Measurement

From Figure 4.6,  $T_{RTD}$  can be found with the RTD properties,

$$T_{RTD} = \frac{\frac{U_T}{(U - U_T) / (R_1 + R_4)} - R_T}{R_{nominal} / R_T} \quad (4-9)$$

where  $U_T$  is the voltage on the RTD, and  $U$  is the voltage of the power supply, and  $R_{nominal}$  is the nominal resistance of the RTD sensor.

### 4.3.2 Test Bed

The pipe was connected directly to a liquid circulator (Figure 4.7, Fisher Scientific Standard Refrigerated Isotemp Baths Circulator, Model 3016S) with a plastic conduit, which is

temperature adjustable and provides a constant flow rate of 15L/min. The pipe was placed horizontally on the table and maintained constant exposure to the room air (See Figure 4-4a). Room temperature was maintained at approximately 23°C. All RTDs were placed in this type of room condition for a period of time (approximately 1 hour) and calibrated prior to the measurement (see Appendix A). The water temperature was measured by a thermometer in the circulator (Figure 4.7).

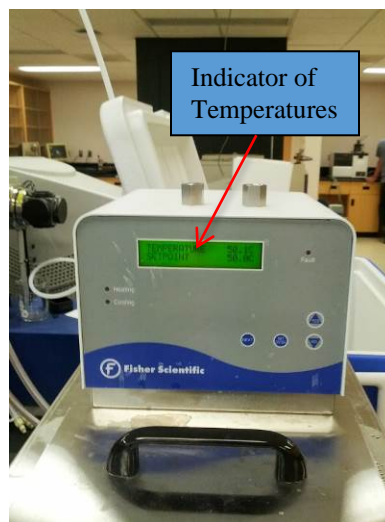


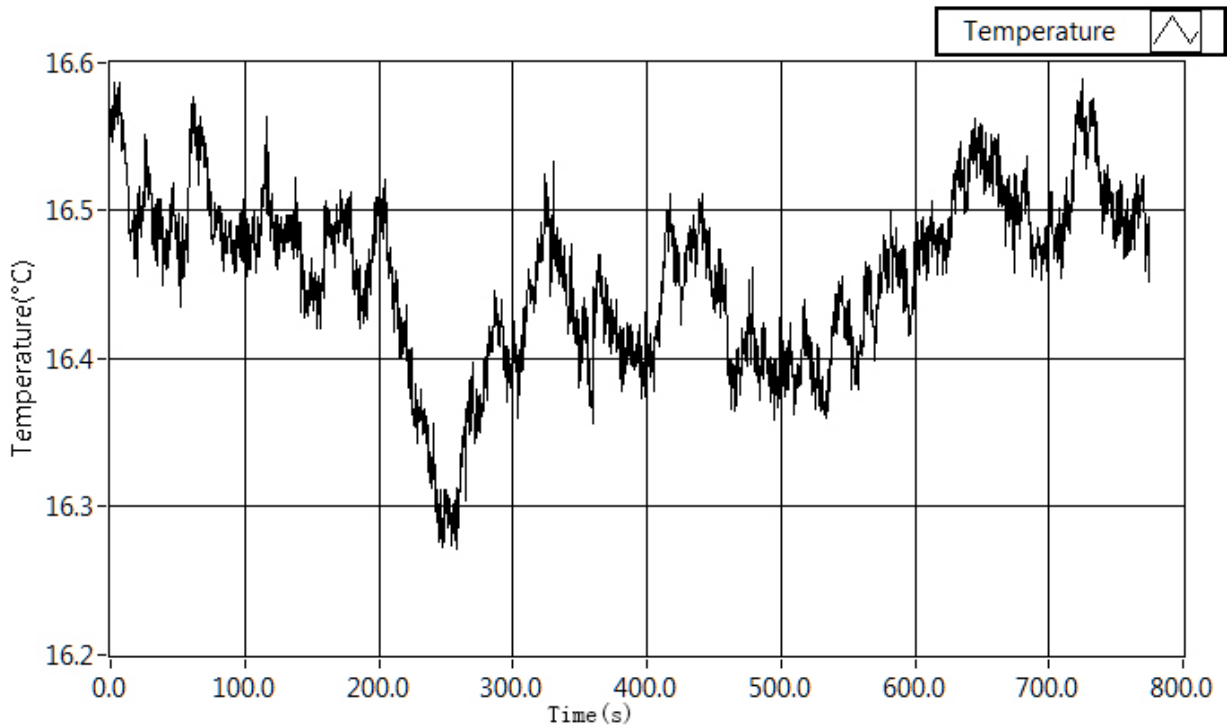
Figure 4.7 Temperature Adjustable Circulator

It is noted that in this experiment, the pressure sensor was not actually put on the inner wall of the pipe due to some unexpected problem related to the availability of the pressure sensor as well as the long manufacturing lead time to make a slot to install the pressure sensor on the inner wall. Though this is an undesired situation to prove the concept of Principle 2, this was acceptable for two reasons. The first reason is that the measurement of the pressure on the inner wall is a common practice in the pipe system, which means that this is highly feasible. The second reason

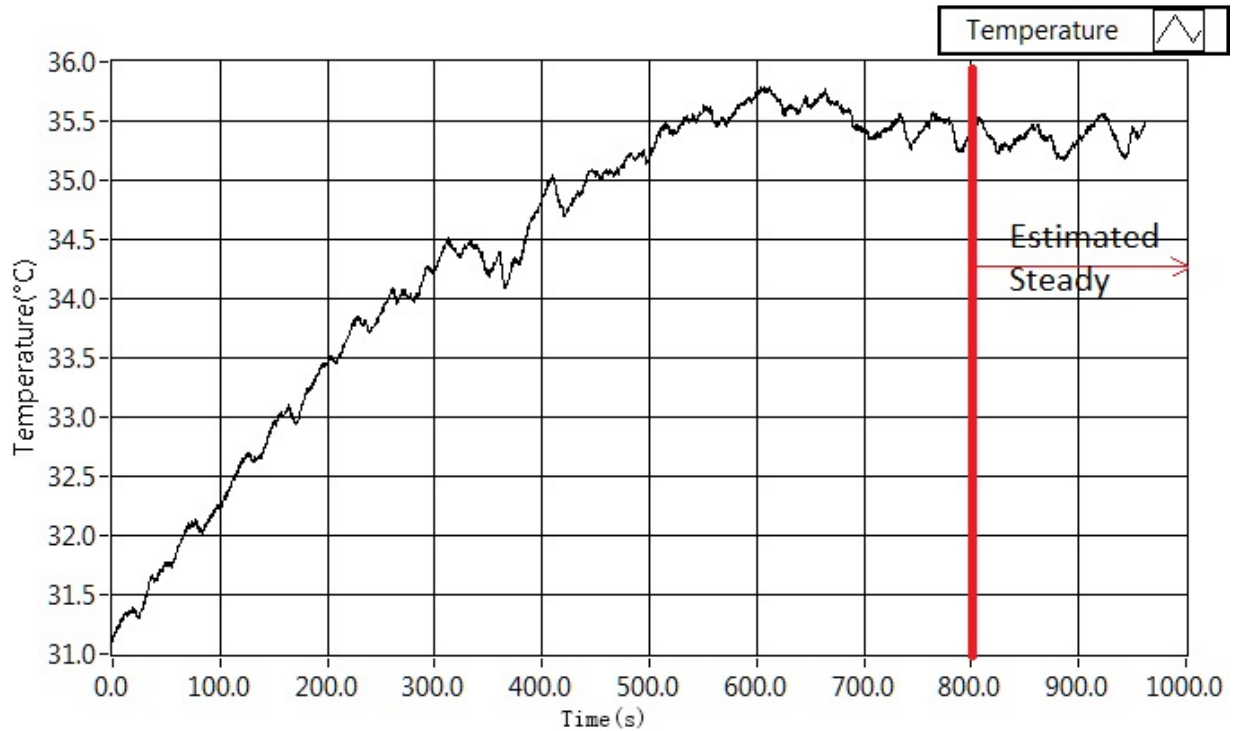
is that the very essence to prove the concept of Principle 2 is really about the feasibility of creating a mathematical model and its inference accuracy.

#### 4.4 Results and Analysis

All laboratory data were collected *in-situ*, and useful information for further analysis was gathered when the fluid was in a steady state (roughly after the 800 seconds of fluid running). This time, which may be called a critical time, was determined through a trial and error process. Figure 4.8 shows the temperature versus time when the temperature was 15°C and 45°C. From the two plots, an estimate of the critical time being 800 seconds was made, in particular from Figure 4.8. It is noted that all of the measurements began to be taken only after this critical time.



(a) RTD Response when the Pump Temperature set at 15°C



(b) RTD Response when the Pump Temperature set at 45°C

Figure 4.8 Temperature Response of the RTD on the Outer Wall

Three measurements of the temperature of water were acquired from the sensor that was on the water circulator. They were used as a reference for testing the accuracy of the inferred temperature from the equations presented before. They were: 5, 10, and 15°C. The temperature of the outer wall of the pipe was measured by the RTD placed on the outer wall. For the three reference temperatures of water, the temperatures on the outer wall were read as: 10, 14, and 16.5°C. In the following, the result of inference of the temperature of water is illustrated.

Table 4-2 and Table 4-3 show the parameters of this particular pipe system. It is noted that the convection coefficient between the air in the room and the outer wall ( $\bar{h}_c$ ), and the convection coefficient between the water and the inner wall of the pipe ( $h_1$ ), are estimated to be 32 and 450, respectively. For details of the estimation, refer to Appendix B.

The heat flux that goes through the wall can be found from Equation (4-8), i.e.,

$$q' = \bar{h}_c D_{pipe} (T_{air} - T_{out}) = 32 \times 0.063 \times (23 - 10) = 26.208 \text{ W/m}$$

The temperature of water can be found from Equation(4-7), i.e.,

$$T_{water} = T_{out} - q' \left( \frac{\ln \frac{D}{d}}{2\pi K} + \frac{1}{h_1 \pi D} \right)$$

$$= 10 - 26.208 \left( \frac{\ln \frac{0.063}{0.05}}{2\pi \times 0.2} + \frac{1}{0.063 \times 450 \times \pi} \right) = 4.886^\circ\text{C}$$

Table 4-4 lists the results of the calculated temperature and measured temperature of water for the three test temperatures (i.e., 5, 10, and 15°C), as well as their relative error.

Table 4-2 Pipe Properties

Outer Diameter (O.D.) M	Inner Diameter (I.D.) m	Length (L) m	Thermal Conductivity (K) W/(m·k)
0.063	0.05	0.317	0.2

Table 4-3 Physical Characteristics of Water at the Atmospheric Pressure

Temperature T °C	Density ρ kg/m <sup>3</sup>	Dynamic Viscosity μ kg/(m·s)	Specific Heat C <sub>p</sub> j/kg	Thermal conductivity K <sub>1</sub> W/(m·k)
5	1000	0.00152	4202	0.5715
10	999.77	0.001308	4192	0.5818
15	999.19	0.001139	4186	0.5917
35	994.08	0.00072	4178	0.6252
45	992.25	0.000596	4180	0.6387

Table 4-4 Results Based on the Estimated Coefficients

<b>Preset Water Temperature</b> $T_{water}^m$ °C	<b>Calculated Water Temperature</b> $T_{water}$ °C	<b>Relative Error</b> (%)
5	5	2.285
10	10	2.285
15	14	7.048

It is noted that there is an inference error on the temperature of water. The inference error may come from two sources. The first source of error is from the sensor on the outer wall. There is an error of 2% with this sensor. This error is transferred to an error of the temperature of water, 2% (see Appendix B). The second source of error is from the sensor used to measure the temperature of air in the room. The estimated error for the measured temperature of air in the room is about 3%, which is translated to the error of 5.14% (see Appendix C). Therefore, the total inference error on the temperature of water is about 7.14%. It is also noted that the sensor to measure the temperature of water (i.e., the reading from the circulator) has the error of 1%. By combining both the inference error and measurement error on the temperature of water, the accuracy of the inference as indicated in Table 4-4 is acceptable

Further, there are errors that come from the model for inferring the temperature of water. The first error may come from air turbulence due to the temperature rise and drop along the pipe. The second error may come from the data processing system including data acquisition board. The third error may come from the radiation heat transfer along the pipe. Therefore, to pursue a more accurate inference result, an improved model with consideration of some of these error sources may worth trying.

## 4.5 Conclusion

This chapter presented a verification of the second principle for OSMS sensors through a case in which both temperature and pressure on a site needed to be measured. This principle states that one signal can be inferred while the other can be measured. Without loss of generality, the temperature signal in this case was considered to be inferred, while the pressure was measured (however, due to some constraints, the pressure sensor was not actually installed). The verification involved testing the accuracy of the temperature inference model. Closely related to this principle, the design for measurement (DFM) philosophy was applied in the design of the test system (i.e., a pipe system with water flowing inside). The result of the verification has clearly shown that (1) the DFM approach is useful, and (2) the second principle in connection with DFM appears valid.

However, the OSMS sensor based on this principle much relies on the availability of the model for inference of the target information. As it is known, any model is built upon a set of assumptions, and the inference accuracy through the model is thus limited.

## CHAPTER 5

### CASE STUDY II: PROOF OF PRINCIPLE 3 FOR OSMS

This chapter describes the second case on the principles for OSMS sensors. The second case study involved acquisition of temperature and pH-value on the same spot simultaneously and was based on Principle 3 of OSMS. In the second case study, there was an accidental discovery of temperature dependency with a carbon nanotube film. This discovery will also be described in this chapter. Section 5.1 presents two types of CNT films to measure temperature: one with random distributed tubes; the other with aligned tubes. Section 5.2 presents the CNT film deposited with PANI capable of measuring pH-value change. Section 5.3 and 5.4 discuss the mechanisms behind the temperature and pH-value measurements with the CNT film. Conclusions are stated in Section 5.5.

#### 5.1 Temperature Measurement with CNT Films

CNT bundles were previously described as exhibiting temperature dependence [23-26], where the temperatures measured under 300K owe to the underlying transducer principle (which is largely based on the CNT intrinsic electrical property). The **hypothesis** in this work was that CNT films might exhibit temperature sensitivity based on the principle of the tube-to-tube network reconfiguration [5-6], potentially being a temperature sensor.

To test this hypothesis, the CNT Films were fabricated by means of the method developed by Miao et al. [27, 28]. The CNTs solution was comprised of a 0.8mg/ml concentration of CNTs

with a 1% wt surfactant sodium dodecylsulfate. The suspension was sonicated and centrifuged for 30 minutes. Then, the solution was coated on the PMMA substrate using a spray gun. Two types of the CNT films were prepared for the experiment. The CNT film of the first type was composed of randomly distributed single-wall carbon nanotubes (SWNT) coated on methylmethacrylate (PMMA). The CNT film of the second type is composed of well-aligned multi-walled carbon nanotubes (MWNTs) coated on PMMA. The detailed procedure of making these films can be found in [29]. Six samples of the CNT films of the first type were fabricated and their information (initial resistance and initial temperature) can be seen from Table 5.1. One sample of the second type was fabricated and it had an initial resistance of 441K $\Omega$  and initial temperature of 21.7°C. A schematic diagram of the CNT film sample is shown in Figure 5.1, where the gold electrode measured the resistivity change of the CNT film when there was an external temperature field on the film.

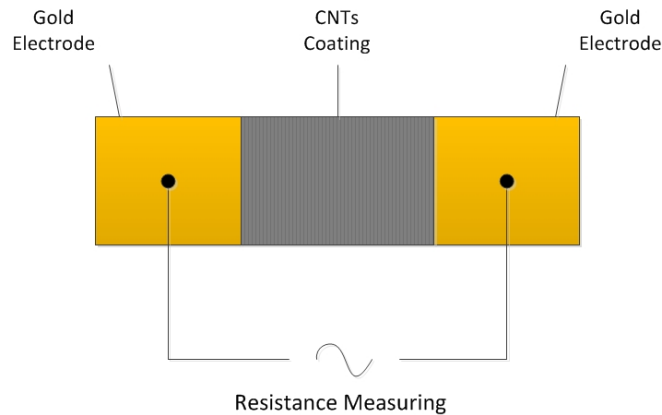


Figure 5.1 Schematic of the tested CNT Film

Different temperatures of the CNT film were achieved with a hotplate (Figure 5.2). The temperature of the hotplate was controlled by a heater (Figure 5.2), ranging from room temperature to 70°C.

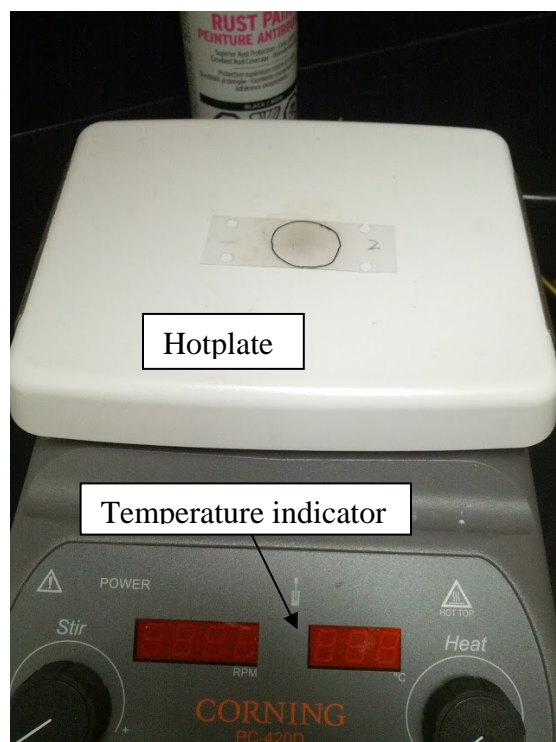


Figure 5.2 Hotplate for Temperature Adjustment

Table 5-1 Resistance of the Samples of the Randomly Distributed CNTs

Randomly Distributed	Sample 1	Sample 2	Sample 3	Sample 4	Sample 5	Sample 6
Initial Resistance (K $\Omega$ )	6.890	2.084	9.97	7.34	6.539	5.518
Temperature via Infrared Thermometer (°C)	22.6	22.6	23.4	23.4	22.2	22.2

The temperature of the film was measured with an infrared thermometer (Cen-Tech, SKU 96451), which was located a certain distance away from the film (Figure 5.4). The infrared thermometer is capable of measuring temperature from 0°C to 100°C with a resolution of 0.1°C and an error bar of 1-2%. The resistance of the film was measured with a digital multimeter (with a resolution of 1 $\Omega$ ). The temperature increment was achieved through the hotplate.

Three experiments were performed: **Experiment 1** (on Sample 1 and Sample 2): to investigate repeatability of the film over time; **Experiment 2** (on Sample 3 and Sample 4): to understand the influence due to a different initial resistance of the film; and **Experiment 3** (on Sample 5 and Sample 6): to study the linearity and hysteresis effect of the film. A film with the well-aligned CNTs was also tested (Figure 5.3). In particular, the direction of the CNTs in the film was perpendicular to the alignment of the probes (Figure 5.3).

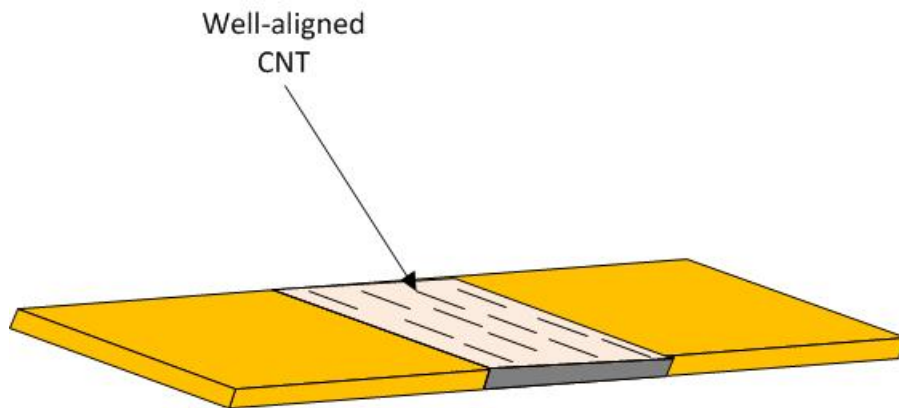


Figure 5.3 Well-aligned CNT Film

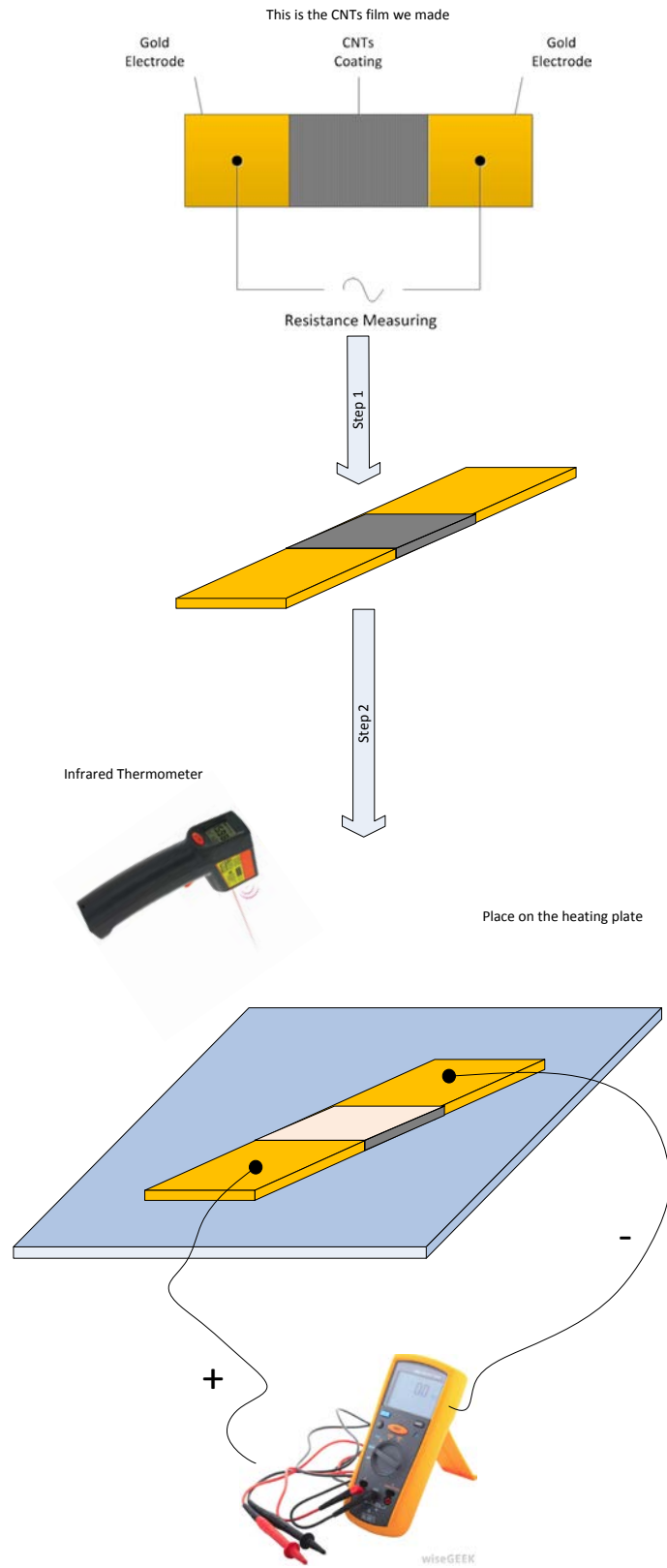


Figure 5.4 Temperature and Resistance Measuring Process

Table 5-2 presents the results of Experiment 1 on Sample 1. That is, the resistance versus temperature on the film. The measurement data was acquired every ten minutes and there were two sets of measurements on the same sample within 24 hours. The second test was conducted 10 hours after the first test under the same external condition. Figure 5.5 is a plot of the results. From Figure 5.5, it can be seen that the film sensor has an excellent linearity and good repeatability (notice: the total error bar on each point on the plot is about 2%, the maximum error between the two test results in Figure 5.5 is less than 2%).

Table 5-2 Tests on Sample 1

Test 1 on Sample 1		Test 2 on Sample 1	
Temperature (°C)	Resistance (KΩ)	Temperature (°C)	Resistance (KΩ)
22.6	6.890	23.0	6.970
28.4	6.670	28.7	6.750
28.8	6.620	31.2	6.690
33.7	6.478	37.8	6.433
37.4	6.353	47.5	6.163
40.9	6.226	50.8	6.090
45.3	6.103	61.4	5.847

Figure 5.5 Relationship between Temperature and Resistance (Sample 1)

Table 5-3 is the result for Sample 2 and Figure 5.6 is a plot of the result. The sample was tested under the same conditions as Sample 1. It can be seen from Figure 5.6 that the repeatability of this sample is much poorer than that of sample 1, but a linear relationship appears to be present between resistance and temperature ( $R^2=0.97, 0.87$ ).

From the results of the two samples, there appears to be a problem regarding stability of the film during fabrication. After the film was made, the structure of the film (i.e., configuration of CNTs) contained internal stress. After the first test was done and the film cooled down to room temperature, and remained at room temperature for some time, the internal stress in the film was released and the mechanical property of the film appeared to stabilize. More tests are needed to confirm this possible issue as this study was limited to two tests.

Table 5-3 Tests on Sample 2

Test 1 on Sample 2		Test 2 on Sample 2	
Temperature (°C)	Resistance (KΩ)	Temperature (°C)	Resistance (KΩ)
22.6	2.084	23.0	1.590
27.8	2.040	28.7	1.498
28.2	2.000	29.4	1.491
32.0	1.958	37.2	1.485
36.2	1.927	40.6	1.483

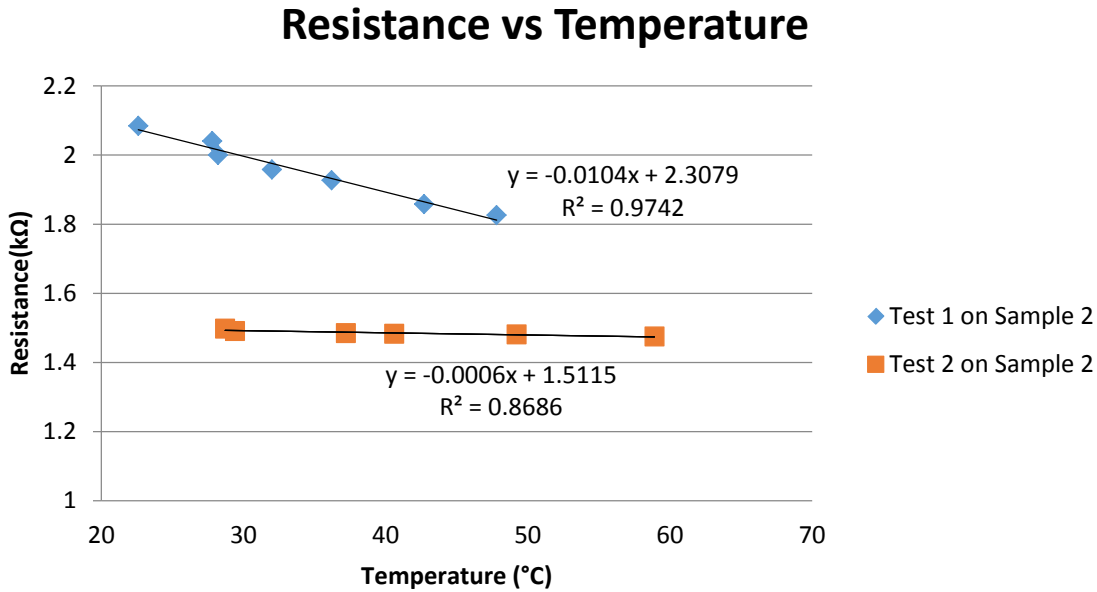


Figure 5.6 Relationship between Temperature and Resistance (Sample 2)

Table 5-4 shows the results of sample 3 and 4. Figure 5.7 is a plot of the result in Table 5-4. The two tests were conducted under the same conditions as Sample 1 and 2. It can be seen from Figure 5.7 that there is a significant influence of the initial resistance of the film over the sensitivity of the film. In particular, the larger that the initial resistance of the film, the higher the sensitivity to temperature.

Table 5-4 Performance of the CNT Films with Different Initial Resistance

Sample 3		Sample 4	
Temperature °C	Resistance(kΩ)	Temperature °C	Resistance(kΩ)
23.4	9.97	23.4	7.34
29.8	9.38	29.2	7
35.6	9.06	34.6	6.82
38.4	8.76	37.3	6.63
42.6	8.39	41.5	6.43
48.6	8.02	47.5	6.24
52.4	7.68	51.8	5.98
57.5	7.38	55.9	5.81
61.4	7.15	59.5	5.65
64.4	6.95	63.4	5.54
69.5	6.81	66.3	5.42

Linearity of Two Different Samples

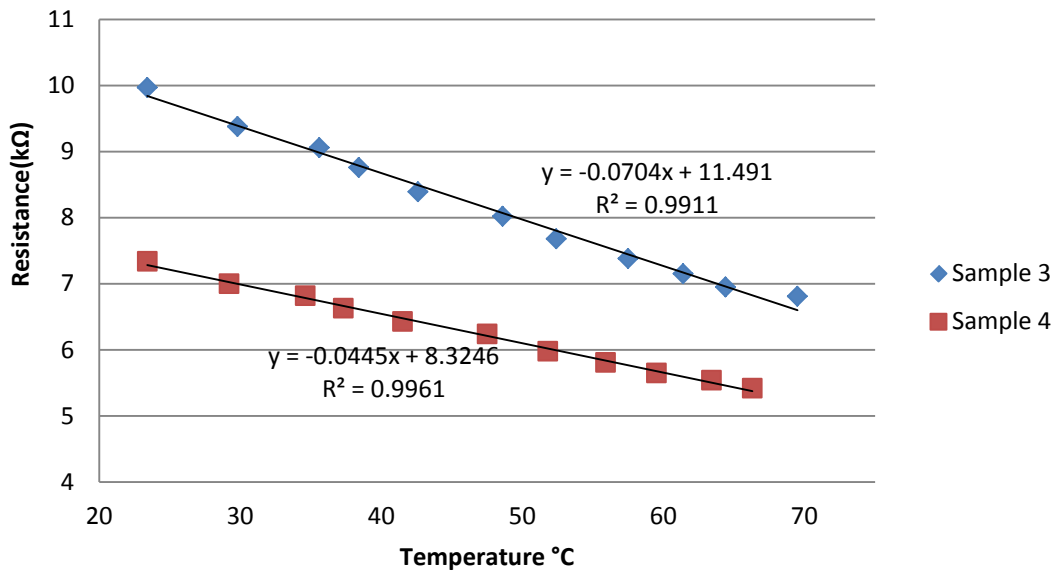


Figure 5.7 Relation between Temperature and Resistance (Samples with Different Initial Resistance)

Table 5-5 and Figure 5.8 show the results of the hysteresis effect and linearity of the film. It can be seen from Figure 5.8 that there was a significant hysteresis effect among the films. The error of the both films is about 0.2°C. This corresponds to a measurement error bar of 2%, which is

acceptable because the sensor error bar (sensor for temperature and sensor for resistance) can reach 2%.

Table 5-5 Samples Subject to Increasing and Decreasing Temperature Field

Sample 5		Sample 6	
Temperature °C	Resistance(kΩ)	Temperature °C	Resistance(kΩ)
22.2	6.539	22.2	5.518
30.5	6.340	29.9	5.381
38.7	6.162	37.6	5.263
41.2	6.119	41.0	5.221
45.4	6.061	44.8	5.185
56.3	5.940	57.4	5.095
64.7	5.899	63.8	5.049
68.4	5.854	69.3	5.015
60.5	6.004	60.0	5.011
56.1	6.212	55.0	5.200
47.7	6.246	47.3	5.312
40.3	6.355	39.5	5.400
31.6	6.543	32.8	5.507
28.0	6.630	27.9	5.591
26.0	6.690	26.9	5.624

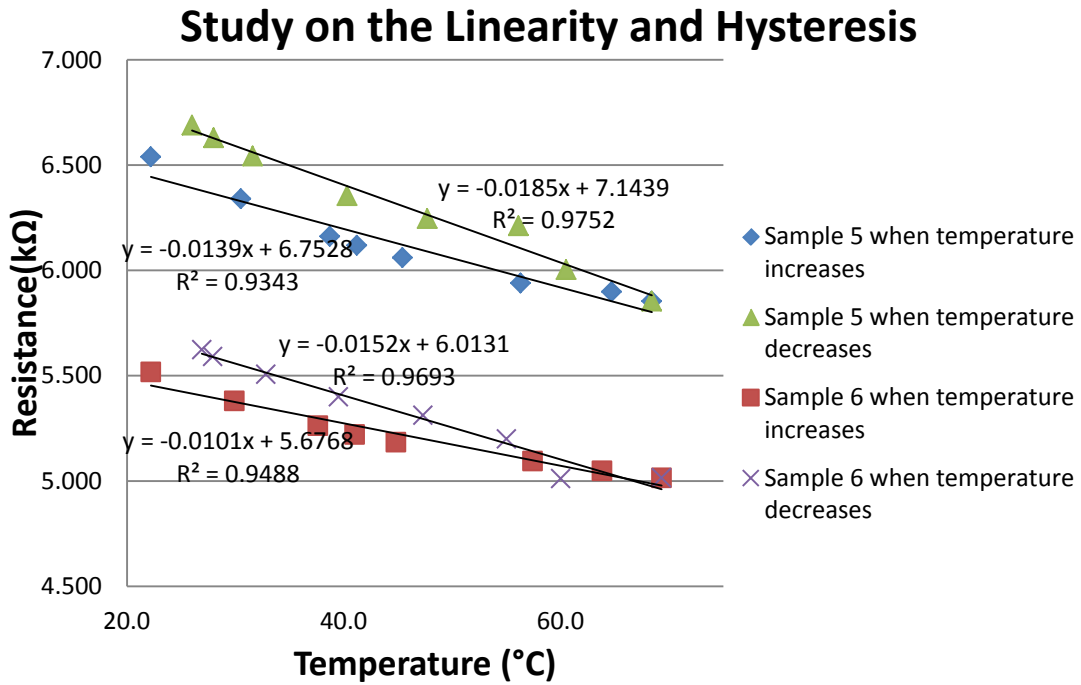


Figure 5.8 Film Performance Regarding Linearity and Hysteresis

Table 5-6 and Figure 5.9 are the results for the well-aligned CNT films, where the hysteresis and linearity are also shown. It can be seen from Figure 5.9 that the repeatability of the film is poor while the sensitivity is quite high.

Table 5-6 Well-aligned CNT film Temperature Performance

Temperature (°C)	Resistance (KΩ)
21.7	441
26.3	430
32.5	418
39.4	404
48.4	393
56.2	387
59.3	382
64.1	380
58.3	383
49.1	388
40.7	396
36.2	401
32.6	406

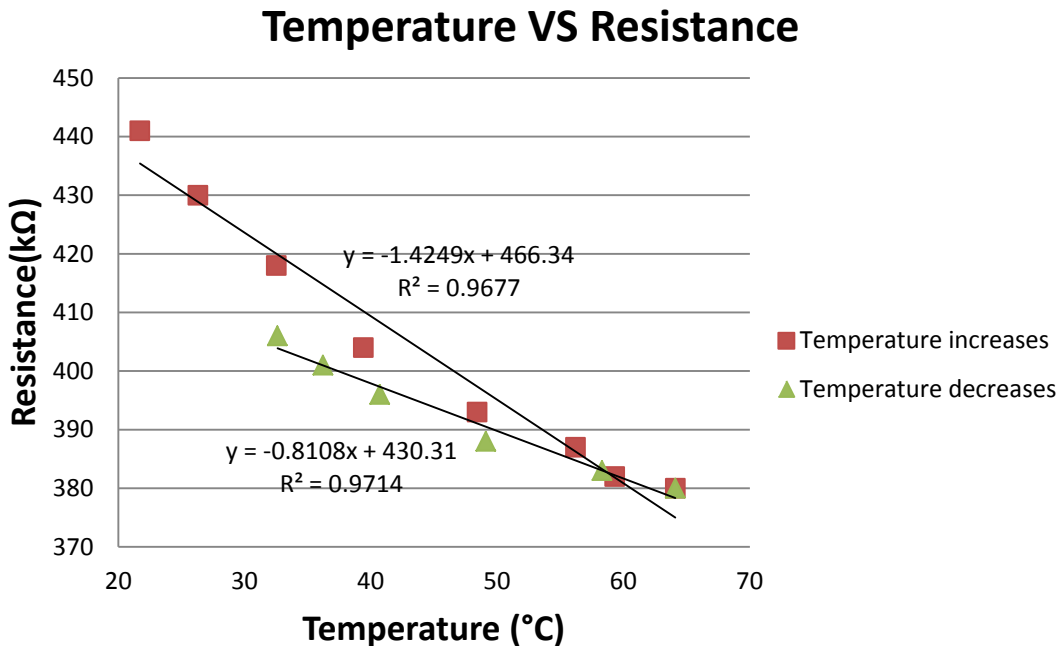


Figure 5.9 Temperature Performance of the Well-aligned CNT Film

## 5.2 pH-value Measurement with the CNT Films

A powder with pH-sensitivity in color change was added onto the aforementioned CNT film. In particular, the powder of Polyaniline (PANI, manufactured by Sigma-Aldrich, Emeraldine bases) was used due to its good conductivity, solubility, and pH-sensitivity shown by color (change from emeraldine base to emeraldine salt, i.e. blue to green) [30]. The deposition of PANI onto the CNT film was achieved with an electrochemical process by following published procedures [31-33]. Hereafter, the resulting composite is called PANI-CNT film.

### 5.2.1 PANI-CNT Film Preparation

The synthesis of PANI-CNT film was based on an electrochemical process. The process consisted of two electrodes, a medium that connected the electrodes, and an external electric energy source that connected the electrodes. Part of a CNT film sample was coated with gold and

served as an electrode (Cathode) (Figure 5.10); the other electrode was a non-CNT PMMA film coated with gold. Sodium Chloride was dissolved into 100 ml solvent, resulting in the solution of Dimethyl sulfoxide (DMSO). The concentration of sodium chloride in the DMSO solution was 5.85%. Mixing 0.5g PANI into the solution results in a final product of PANI solution, in which blue emeraldine base was charged with sodium. It is noted that this blue solution served as a medium (Figure 5.11). An electrochemical cell device was then built as shown in Figure 5.12. An external electric energy of 0.75 V was added to connect the two electrodes (Figure 5.12). It is noted that sodium salt was used as an electrolyte. Emeraldine is an oxidized state of PANI in the solution medium. DC current was applied to the two electrodes, resulting in the cathode (CNT networks) charged with electrons, which attracted the PANI to the surface and formed a layer on the cathode (i.e., CNT film).

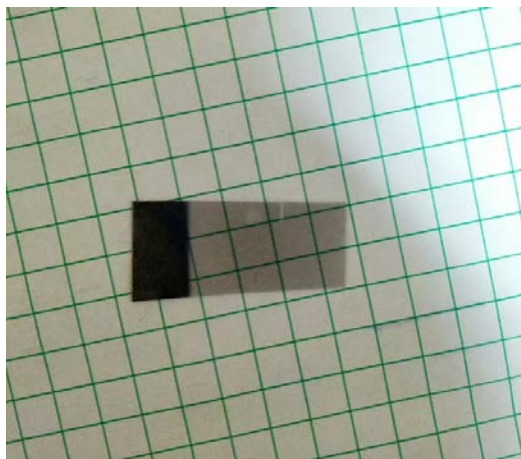


Figure 5.10 CNT Film Sample Prepared for Deposition



Figure 5.11 Polyaniline Solution Prepared for Electrochemical Deposition

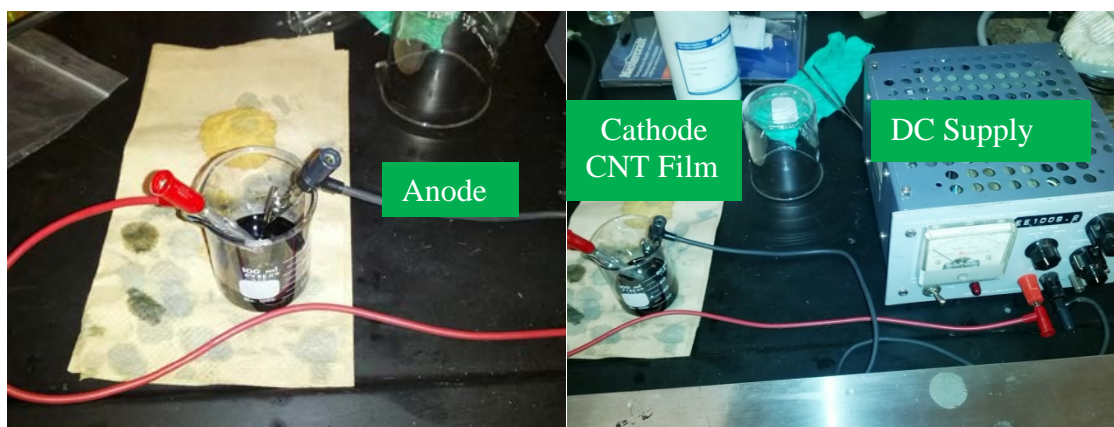


Figure 5.12 Building of Electrochemical Cell

Due to the high resistance of the CNT film, the current for the system was expected to be fairly small. A relatively longer deposition time (15 minutes for our experiments) was therefore taken. When the deposition on the cathode was finished, the films were dried out naturally at room temperature. Figure 5.13 illustrates several PANI-CNT film prototypes.

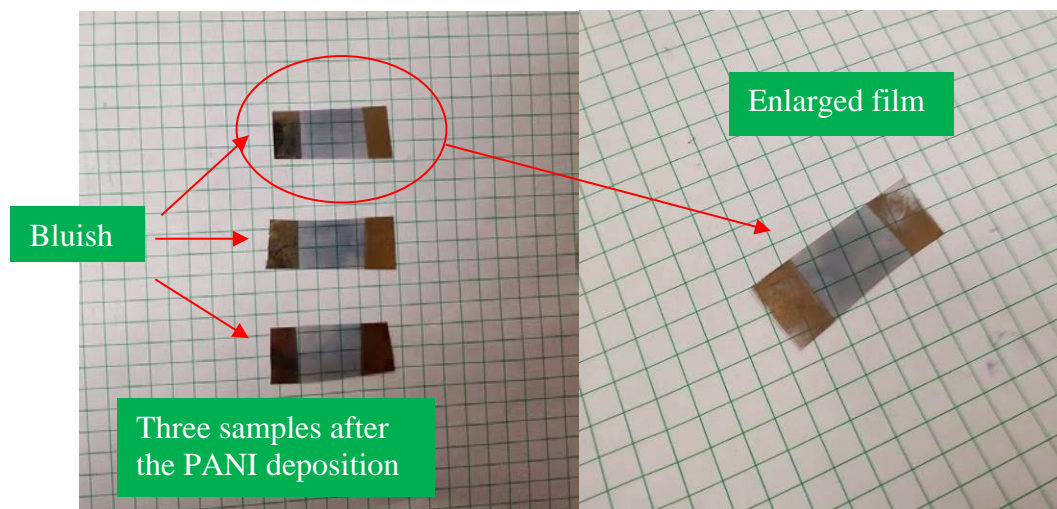


Figure 5.13 Prototypes for Temperature Measurement and pH Detection

### 5.2.2 pH-value and Temperature Measurement

Sulfuric Acid (10%) was prepared as the verification liquid for pH-detection. It is noted that in this study, there was no attention to quantify the pH-value measurement and the study was restricted to examining whether the sensor was sensitive to a change of acidic state of liquid. The acid was dipped onto the PANI-CNT film. Figure 5.14 shows the result after one part of the film was dipped into the acid. From Figure 5.14, it can be seen that the layer was rather thin yet visible to the naked eye. It is noted that in this study only two states of pH were considered as a pilot trial to see if the concept worked.

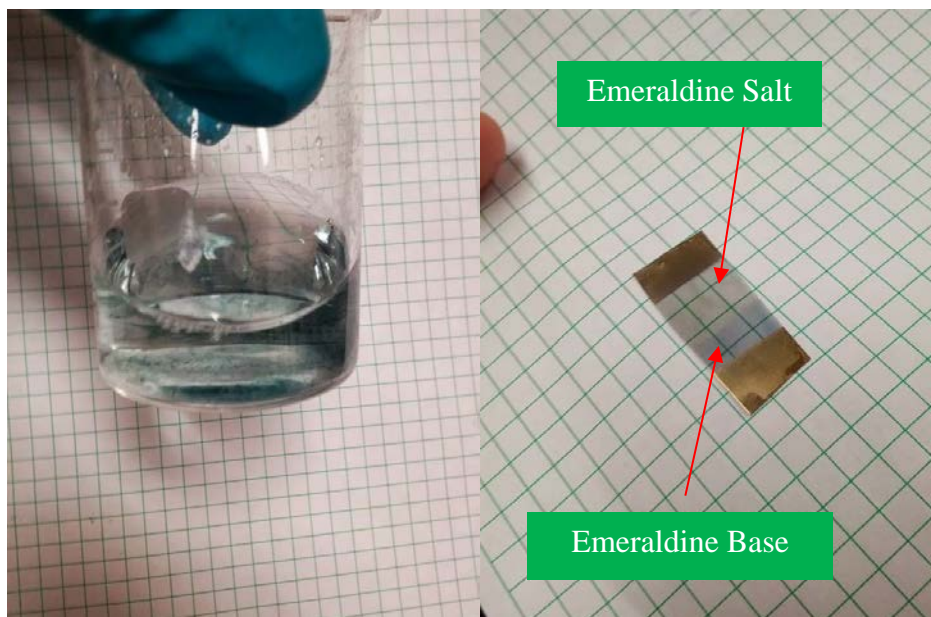


Figure 5.14 Results after the Acid Doping

To demonstrate the temperature-resistance performance after the PANI deposition, one film was further tested for the temperature dependency of the film (Figure 5.15). Table 5-7 gives the result of the temperature versus resistance of the film. Figure 5.16 is a plot of the result.



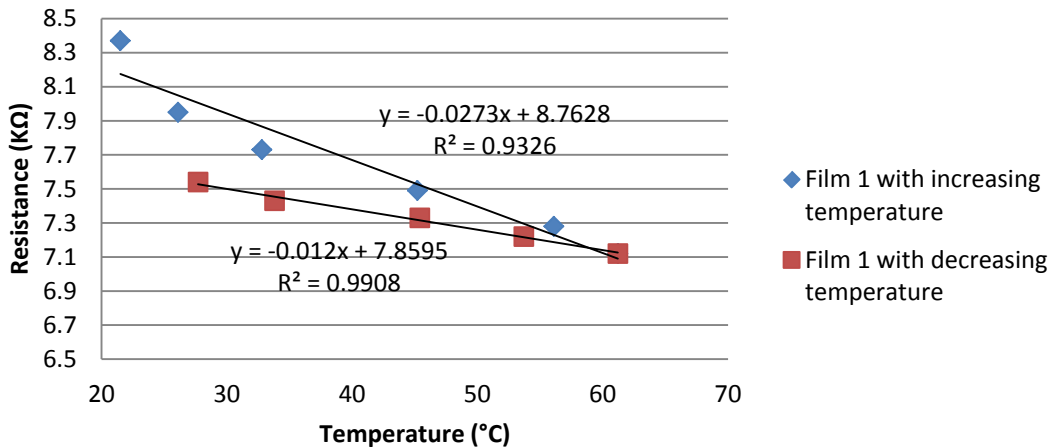
Figure 5.15 Test of Temperature Dependency of the CNT Film Deposited with Polyaniline

After testing, the PANI structure appeared to be stable (Figure 5.15). The resistance under the temperature field also showed good linearity. It can also be seen from Figure 5.16 that the temperature-resistance relation has a good linearity, but the PANI-CNT seems to have more hysteresis than the CNT film without PANI deposition. With PANI deposition, the comeback line (the line when temperature drops) deviated a greater amount from the line when temperature increased than with the non-deposited film.

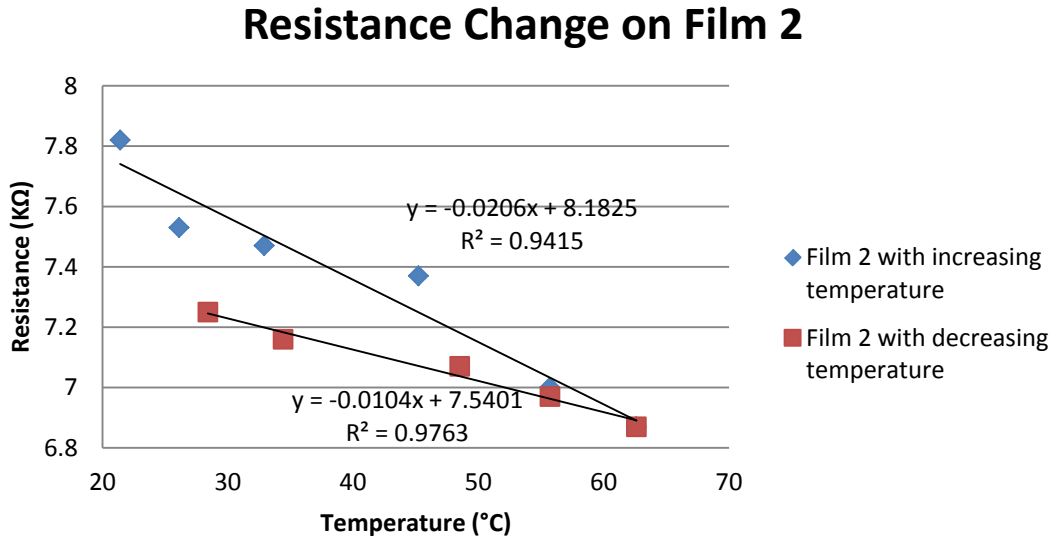
Table 5-7 Temperature Dependence of the Deposited Films

Film 1		Film 2	
Temperature (°C)	Resistance (KΩ)	Temperature (°C)	Resistance (KΩ)
21.5	8.37	21.4	7.82
26.1	7.95	26.1	7.53
32.8	7.73	32.9	7.47
45.2	7.49	45.2	7.37
56.1	7.28	55.7	7.00
61.2	7.12	62.6	6.87
53.7	7.22	55.7	6.97
45.4	7.33	48.5	7.07
33.8	7.43	34.4	7.16
27.7	7.54	28.4	7.25

### Resistance Change on Film 1



(a) Film 1 Resistance against Temperature



(b) Film 2 Resistance against Temperature

Figure 5.16 Resistance Change of Two PANI-modified Films

### 5.3 Temperature Dependence of the CNT Film without PANI: Discussion

The linear response of CNT films above room temperature has not been reported in literature. In current literature, it is well known that the CNT network or film has a temperature dependency property, with temperature needing to be below room temperature. In the following section, the plausible mechanism for the CNT film developed in this thesis is explored (the film without PANI is considered).

Three mechanisms regarding the temperature-resistance effect of the CNT networks are reported in the literature: (1) contact tunneling resistance in tubes with defects [34, 35]; (2) tube-tube interactions [36-38]; and (3) Variable-range Hopping (VRH) conduction [34, 38, 39].

The tunneling conduction was first proposed by Sheng [40] for disordered materials. It stated that the conduction between nano-materials barriers could be activated at a certain level of energy. This was further proved to be applicable for Single-walled CNT networks [41], where metallic and semi-conductive tubes were both present. They possessed metal-metal junction (M-M), semiconductive-semiconductive junction (S-S), and metal-semiconductive junction (Skottchy barrier), even though the pathway between metallic CNTs dominated the mechanism. It was also reported that a U-shaped temperature dependence of resistivity was observed in the glass film (Figure 5.17). However, this phenomenon has not been observed in the CNT film of this thesis. Therefore, it is unlikely that this mechanism dominated the temperature-dependency property of the CNT film of this thesis.

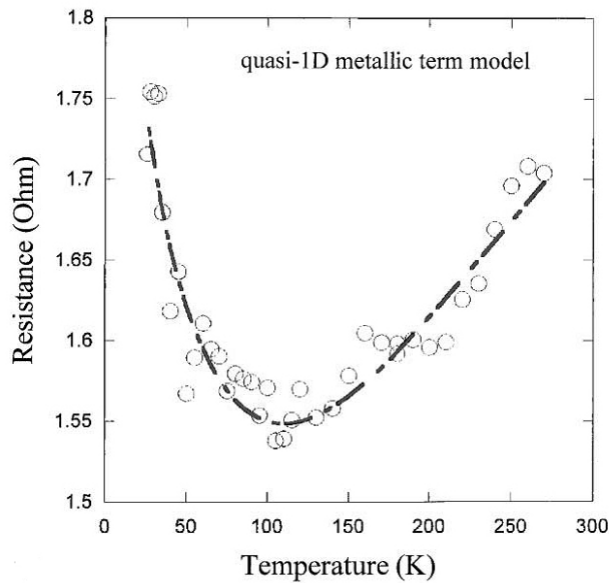


Figure 5.17 U-shaped Temperature Dependence [34]

Li et al. [42] reported that a positive thermal coefficient (Figure 5.18) from a Polyvinylidene fluoride (PVDF) based CNT composites was due to the different thermal expansion coefficients between the CNTs and the polymer. This mechanism was not readily applied to the CNT film of

this thesis because the behavior of the film of this thesis showed a monotonic decreasing trend (i.e., when temperature is up the resistance is down).

From the results from the ‘bulky paper’—thin mats of entangled single-walled carbon nanotubes (deposited on transparent substrates such quartz and sapphire) [35]—, the CNT film of this thesis exhibited a rather similar effect to one of the films (Figure 5.19) within the testing temperature range, in particular the performance of the second cycle indicated in Figure 5.19. This might indicate that the CNT films could be undergoing a similar physical condition to the second cycle. However, it does not necessary mean that the structure of both films are alike.

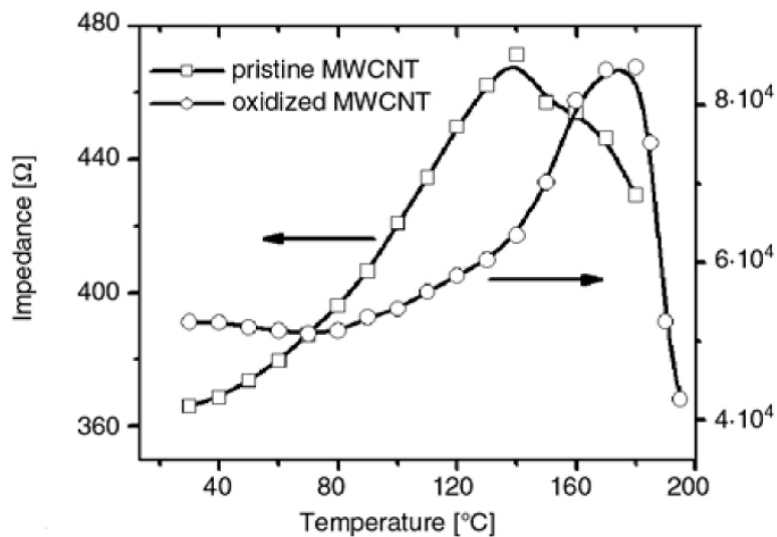


Figure 5.18 Temperature Dependence of Pristine and Oxidized CNT Composites [42]

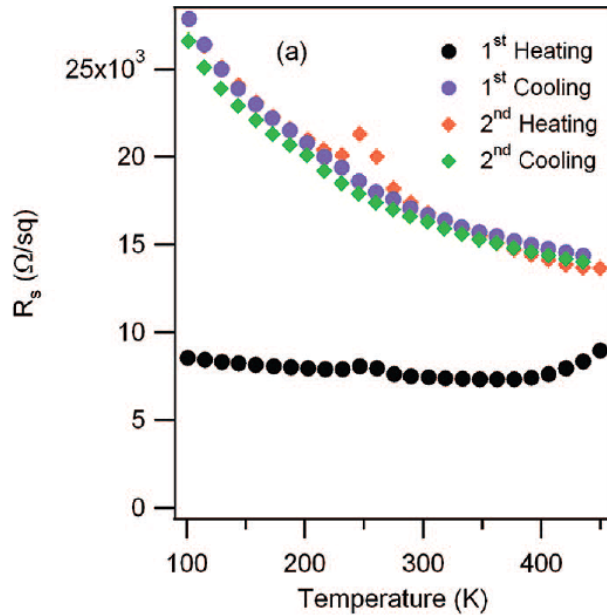


Figure 5.19 Temperature-dependent Resistivity of an Unintentionally Doped Bulk SWNT Film for Two Heating and Cooling Cycles [35]

The film with CNTs aligned by a magnetic approach fabricated in this thesis also showed a good linearity over temperature range from room temperature to 70°C. A surprising discovery was that the resistance drop was even more substantial than that of the randomly distributed CNT film. Because the resistance measurement was perpendicular to the tube alignment direction, it was less likely that the polymer expansion dominated the temperature-resistance relation of the film in this thesis. The results are similar to the effect of the carbon nanotubes composite [43]. If the thermal expansion is the cause of this effect, then the number of junctions between the tubes should be reduced when temperature increases and further resistance should also increase. As shown before, the fact that the well-aligned CNT film of this thesis exhibited a resistance decreasing behavior when temperature increased (Figure 5.9), the applicability of the theory proposed in [42] to the film of the present study (including both the randomly distributed CNT film and well-aligned CNT film) is invalid.

Regarding why the sensitivity of the well-aligned CNT film (resistance direction is perpendicular to alignment direction) was higher than that of randomly distributed CNT film, the cause could be due to the strain-resistance dependency property of the same film studied by Miao [27]. That is, when temperature increased the number of junctions also increased and thus the resistance reduced. It is noted that in the literature, there is a theory that oxygen doping may be a cause of this phenomenon (in fact, oxygen doping was even considered as a cause for the temperature dependency property with randomly distributed CNT films) [21]. However, this theory is inconsistent with the CNT film developed in this thesis.

Above all, the principle that governs the temperature-resistance property with the CNT film (regardless of the CNT distribution configuration and with temperature range of room temperature to 70°C) is speculative. Perhaps the films used in this thesis might have a tube-to-tube configuration change combined with the tunneling conduction (minor). This is important because when temperature increases, more tube-to-tube junctions occur and conductivity increases. Oxygen doping may be present and contribute to this phenomenon. However, it is likely that oxygen doping may be a disrupting factor for linearity because the amount of oxygen is temperature dependent. Further, by combining the knowledge reported in literature regarding temperature-resistance effect of the CNT film (dropped over electrode arrays on a glass substrate) [34], it appears that at a low temperature range (below room temperature) the tunneling conduction principle dominated the effect. This is perhaps because such a temperature is too low to incur deformation that results in the change of tube-to-tube junction configuration. But, when the temperature increased above room temperature, a temperature induced force was sufficiently large to cause changes of the tube-to-tube junction configuration.

#### **5.4 Sensitivity of the PANI-CNT film to pH: Discussion**

Due to the chemical instability of emeraldine base in air, long-term preservation has been out of the question. However, it was found that the PANI deposition was highly reproducible even if the film had been in contact with the acid. Theoretically, both emeraldine base and salts can be removed thoroughly from CNT networks by reversing the potential. The deposition could be time-consuming (depending on the resistivity of the CNT network and the applied voltage) but the reproduction process was non-destructive.

It was odd that after the PANI deposition, the temperature dependence property did not differ from the original film (i.e., the film without PANI) and maintained a reasonable performance. The possible assumption is that the CNT network structure was not significantly affected by the PANI.

#### **5.5 Conclusion**

The prototypes of the CNT films (including both well-aligned and randomly distributed ones) have been developed and are able to sense both temperature and pH-value change). In particular, the temperature dependency is more likely to be a promising property with excellent linearity behavior. Detection of the pH change has also demonstrated that the CNT network is rather configurable and versatile, although it may not appear as robust as anticipated. Great potentials for the future development lie in the various designs and modifications to the CNT(s) network.

## CHAPTER 6 CONCLUSIONS AND RECOMMENDATIONS

The final chapter outlines the overview of the entire work and plausible conclusions that can be drawn from the research. Contributions of the study to the respective field will also be discussed as well as potential future directions of work.

### **6.1 Overview and Conclusion**

The study presented in this thesis is motivated by the need to enhance sensing capabilities in a context where a large number of sensors are needed. This need leads to the idea of having one sensor to obtain multiple signals at the same place and same time. Coincidentally, this idea is consistent with the biological systems such as human system, where at one place, a dozen of signals are acquired.

Driven by the above idea, two objectives are proposed for the present study and are restated here:

- Objective 1: Investigate the governing principle of the OSMS. The governing principle means the principle underlying an OSMS sensor to acquire two signals at the same site and same time (SSST). Such a principle can also be viewed as the transducer principle for OSMS sensors.
- Objective 2: Develop two case studies to demonstrate the validity of the principles proposed in Objective 1. Signals in this study are pressure, temperature, and pH value.

With some generalization of the idea of one sensor for multi-signals, relevant developments in literature are reviewed and analyzed in Chapter 2. This has guided the proposal of three principles of OSMS sensors. Principle 1: Acquiring Multiple Signals through a stem signal; Principle 2: One Signal Inference and One Signal Measurement; and Principle 3: Acquiring Multiple Signals through a Multi-transducer structure.

Chapter 4 and Chapter 5 presented two case studies that explore the second and third principles.

This research led to the following conclusions:

1. The idea of a OSMS sensor is valid. The three principles appear to provide a fundamental governing guideline for designing such sensors.
2. The idea of Design for Modeling (DFM), in conjunction with the second principle of OSMS sensors, is promising.
3. The proposed new sensor that can measure both temperature and pH is promising.
4. The proposed new transducer for temperature measurement has high potential.

## **6.2 Contributions**

The main contributions of this study are in developing multi-signal acquisition theory, in which the first contribution lies in the idea of multi-signal sensors; the second contribution lies in the idea of design for modeling (DFM).

To the best of the researchers knowledge, the concept of one sensor for multi-signals (OSMS) has never been raised in the sensor literature. The conventional approach to OSMS places two sensors side-by-side on one place. The conventional approach is limited by space and

interference. The three principles for OSMS sensors have a transformative advancement over this conventional approach, and they are perhaps the first comprehensive theory for sensors to acquire multi-signals at the same site and same time.

The concept of DFM is novel in the sensor design literature. Conventionally, sensor design focuses on the selection of a proper transducer and optimization of a transducer structure.

The study has also discovered a new transducer principle with the CNT film from room temperature to 70-Celsius degrees. This sensor had a high resolution of up to 0.5°C and good flexibility against multiple types of surfaces. This is due to the underlying material and structure of carbon nanotubes. The scientific reason for this new transducer principle is also proposed.

### **6.3 Future Work**

This section presents a discussion of some limitation in this study and sheds some light on the directions for possible future work on OSMS technology. The first limitation lies in that the CNT film prototype showed a poor repeatability in temperature measurement and has not achieved measurement of pH-value. It is unclear what dominant factor was responsible for the quality of the signals from the temperature sensor. Additionally, the preservation of film appears to be another critical problem as the properties of PANI were subject to air; especially regarding the which color gradually wore over time and resulting in the indicator for hydrogen ion existence being no longer visible. It has not been investigated that the film is still sensitive to pH value change after the exposure, but it is advisable to remove the hydrogen after use and store the film in an airtight container for preservation or make an image of it for a persistent storage.

Under many circumstances, more tests are required to improve the quality of the CNT film and to optimize the CNT film in terms of its repeatability and linearity. The mechanism behind the PANI-CNT film remains to be confirmed.

## LIST OF REFERENCES

- [1] H. Salem. (2006) Middleware: Middleware Challenges and Approaches for Wireless Sensor Networks. Available: <http://doi.ieeecomputersociety.org/10.1109/MDSO.2006.19>
- [2] M. Kochhal, L. Schwiebert, and S. Gupta, "Integrating sensing perspectives for better self organization of ad hoc wireless sensor networks," *Journal of Information Science and Engineering*, vol. 20, pp. 449-475, May 2004.
- [3] K. Romer and F. Mattern, "The design space of wireless sensor networks," *Ieee Wireless Communications*, vol. 11, pp. 54-61, Dec 2004.
- [4] H. N. SEGALL, "How Korotkoff, the surgeon, discovered the auscultatory method of measuring arterial pressure," *Annals of Internal Medicine*, vol. 83, pp. 561-562, 1975.
- [5] Y. Lin and W. J. Zhang, "Towards a novel interface design framework: function–behavior–state paradigm," *International Journal of Human-Computer Studies*, vol. 61, pp. 259-297, 9// 2004.
- [6] Y. L. Hongjie Leng, "A MEMS/NEMS sensor for human skin temperature measurement," *Smart structures and Systems*, 2010.
- [7] Y. Lin, H. Leng, G. Yang, and H. Cai, "An Intelligent Noninvasive Sensor for Driver Pulse Wave Measurement," *Sensors Journal, IEEE*, vol. 7, pp. 790-799, 2007.
- [8] H. Leng and Y. Lin, "From human skin to Nano-Skin: an experimental study on human skin temperature measurement," *International Journal of Smart and Nano Materials*, vol. 2, pp. 78-91, 2011.
- [9] M. G. Xu, J. L. Archambault, L. Reekie, and J. P. Dakin, "Discrimination between strain and temperature effects using dual-wavelength fibre grating sensors," *Electronics Letters*, vol. 30, pp. 1085-1087, 1994.
- [10] J. Shi, S. Xiao, M. Bi, L. Yi, and P. Yang, "Discrimination between strain and temperature by cascading single-mode thin-core diameter fibers," *Appl Opt*, vol. 51, pp. 2733-8, May 10 2012.
- [11] H. J. Patrick, G. L. M. Williams, A. D. Kersey, J. R. Pedrazzani, and A. M. Vengsarkar, "Hybrid fiber Bragg grating/long period fiber grating sensor for strain/temperature discrimination," *Photonics Technology Letters, IEEE*, vol. 8, pp. 1223-1225, 1996.
- [12] B.-O. Guan, H.-Y. Tam, H. L. W. Chan, C.-L. Choy, and M. S. Demokan, "Discrimination between strain and temperature with a single fiber Bragg grating," *Microwave and Optical Technology Letters*, vol. 33, pp. 200-202, 2002.
- [13] C. Grimes, C. Mungle, K. Zeng, M. Jain, W. Dreschel, M. Paulose, *et al.*, "Wireless Magnetoelastic Resonance Sensors: A Critical Review," *Sensors*, vol. 2, pp. 294-313, 2002.
- [14] M. K. Jain and C. A. Grimes, "A wireless magnetoelastic micro-sensor array for simultaneous measurement of temperature and pressure," *Magnetics, IEEE Transactions on*, vol. 37, pp. 2022-2024, 2001.
- [15] I. Graz, M. Krause, S. Bauer-Gogonea, S. Bauer, S. P. Lacour, B. Ploss, *et al.*, "Flexible active-matrix cells with selectively poled bifunctional polymer-ceramic nanocomposite for pressure and temperature sensing skin," *Journal of Applied Physics*, vol. 106, pp. -, Aug 1 2009.
- [16] I. N. K. Ivanov, TN, US), Geohegan, David Bruce (Knoxville, TN, US), "CARBON NANOTUBE TEMPERATURE AND PRESSURE SENSORS," United States Patent, 2011.

- [17] X. Wu, W. Zhang, R. Sammynaiken, Q. Meng, D. Wu, Q. Yang, *et al.*, "Measurement of low concentration and nano-quantity hydrogen sulfide in sera using unfunctionalized carbon nanotubes," *Measurement Science and Technology*, vol. 20, p. 105801, 2009.
- [18] J. E. Zhan, "Fundamental study of measurement of low concentration hydrogen sulfide in sera using carbon nanotube," University of Saskatchewan, 2010.
- [19] X. Wu, R. Sammynaiken, W. Zhang, D. Wu, Q. Yang, W. Yang, *et al.*, "Measurement of low concentration and nano-quantity hydrogen sulfide in aqueous solution: measurement mechanisms and limitations," *Measurement Science and Technology*, vol. 18, p. 1315, 2007.
- [20] N. P. Suh, "Axiomatic design theory for systems," *Research in engineering design*, vol. 10, pp. 189-209, 1998.
- [21] W. S. Janna, *Engineering Heat transfer*, Third Edition ed.: CRC Press, 2009.
- [22] N. Instruments. (2013). *Choosing an RTD or Thermistor Measurement System*. Available: <http://www.ni.com/white-paper/3643/en>
- [23] F. Huang, K. T. Yue, P. Tan, S.-L. Zhang, S. Zujin, X. Zhou, *et al.*, "Temperature dependence of the Raman spectra of carbon nanotubes," *Journal of Applied Physics*, vol. 84, pp. 4022-4024, 1998.
- [24] C. Y. Kuo, C. L. Chan, C. Gau, C. W. Liu, S. H. Shiau, and J. H. Ting, "Nano Temperature Sensor Using Selective Lateral Growth of Carbon Nanotube Between Electrodes," *Nanotechnology, IEEE Transactions on*, vol. 6, pp. 63-69, 2007.
- [25] K. K. Nanda, P. Mahanandia, and L. T. Singh, "Possible application of carbon nanotube bundles for low temperature sensing," *Review of Scientific Instruments*, vol. 79, May 2008.
- [26] A. Di Bartolomeo, M. Sarno, F. Giubileo, C. Altavilla, L. Iemmo, S. Piano, *et al.*, "Multiwalled carbon nanotube films as small-sized temperature sensors," *Journal of Applied Physics*, vol. 105, pp. 064518-064518-6, 2009.
- [27] Y. Miao, Q. Yang, L. Chen, R. Sammynaiken, and W. J. Zhang, "Modelling of piezoresistive response of carbon nanotube network based films under in-plane straining by percolation theory," *Applied Physics Letters*, vol. 101, pp. -, 2012.
- [28] Y. Miao, Q. Q. Yang, R. Sammynaiken, W. J. Zhang, J. Maley, and G. Schatte, "Influence of aligned carbon nanotube networks on piezoresistive response in carbon nanotube films under in-plane straining," *Applied Physics Letters*, vol. 102, pp. -, 2013.
- [29] Y. P. Miao, "A New Strain Sensor Based on Pure CNT Films," Master of Science, Department of Mechanical Engineering, University of Saskatchewan, 2010.
- [30] W. J. Feast, J. Tsibouklis, K. L. Pouwer, L. Groenendaal, and E. W. Meijer, "Synthesis, processing and material properties of conjugated polymers," *Polymer*, vol. 37, pp. 5017-5047, 10// 1996.
- [31] R. K. Nagarale, G. S. Gohil, V. K. Shahi, G. S. Trivedi, and R. Rangarajan, "Preparation and electrochemical characterization of cation- and anion-exchange/polyaniline composite membranes," *Journal of Colloid and Interface Science*, vol. 277, pp. 162-171, 9/1/ 2004.
- [32] M. Özden, E. Ekinici, and A. E. Karagoezler, "Electrochemical preparation and sensor properties of conducting polyaniline films," *Turkish Journal of Chemistry*, vol. 23, pp. 89-98, 1999.
- [33] S. Dhawan and D. Trivedi, "Preparation of conductive polyaniline solutions for electronic applications," *Bulletin of Materials Science*, vol. 12, pp. 153-157, 1989.

- [34] M. Shiraishi and M. Ata, "Conduction mechanisms in single-walled carbon nanotubes," *Synthetic Metals*, vol. 128, pp. 235-239, May 10 2002.
- [35] T. M. Barnes, J. L. Blackburn, J. van de Lagemaat, T. J. Coutts, and M. J. Heben, "Reversibility, dopant desorption, and tunneling in the temperature-dependent conductivity of type-separated, conductive carbon nanotube networks," *Acs Nano*, vol. 2, pp. 1968-1976, Sep 2008.
- [36] M. S. Fuhrer, J. Nygård, L. Shih, M. Forero, Y.-G. Yoon, M. S. C. Mazzoni, *et al.*, "Crossed Nanotube Junctions," *Science*, vol. 288, pp. 494-497, April 21, 2000 2000.
- [37] S. I. Cha, K. T. Kim, K. H. Lee, C. B. Mo, Y. J. Jeong, and S. H. Hong, "Mechanical and electrical properties of cross-linked carbon nanotubes," *Carbon*, vol. 46, pp. 482-488, Mar 2008.
- [38] Y. R. Lai, K. F. Yu, Y. H. Lin, J. C. Wu, and J. J. Lin, "Observation of fluctuation-induced tunneling conduction in micrometer-sized tunnel junctions," *Aip Advances*, vol. 2, Sep 2012.
- [39] A. B. Kaiser, G. C. McIntosh, K. Edgar, J. L. Spencer, H. Y. Yu, and Y. W. Park, "Some problems in understanding the electronic transport properties of carbon nanotube ropes," *Current Applied Physics*, vol. 1, pp. 50-55, Jan 2001.
- [40] P. Sheng, "Fluctuation-Induced Tunneling Conduction in Disordered Materials," *Physical Review B*, vol. 21, pp. 2180-2195, 1980.
- [41] Z. Yao, H. W. C. Postma, L. Balents, and C. Dekker, "Carbon nanotube intramolecular junctions," *Nature*, vol. 402, pp. 273-276, 1999.
- [42] Q. Li, Q. Z. Xue, X. L. Gao, and Q. B. Zheng, "Temperature dependence of the electrical properties of the carbon nanotube/polymer composites," *Express Polymer Letters*, vol. 3, pp. 769-777, Dec 2009.
- [43] Z. Ounaies, C. Park, K. E. Wise, E. J. Siochi, and J. S. Harrison, "Electrical properties of single wall carbon nanotube reinforced polyimide composites," *Composites Science and Technology*, vol. 63, pp. 1637-1646, 8// 2003.
- [44] T. E. toolbox. *Convective Heat Transfer*. Available: [http://www.engineeringtoolbox.com/convective-heat-transfer-d\\_430.html](http://www.engineeringtoolbox.com/convective-heat-transfer-d_430.html)

## APPENDIX A LABVIEW CONFIGURATIONS

### **A.1 BASICS OF LABVIEW SETUP**

Appendix A.1 shows the basic interface, blocks, and corresponding setups of Labview. Critical values are given in the diagrams.

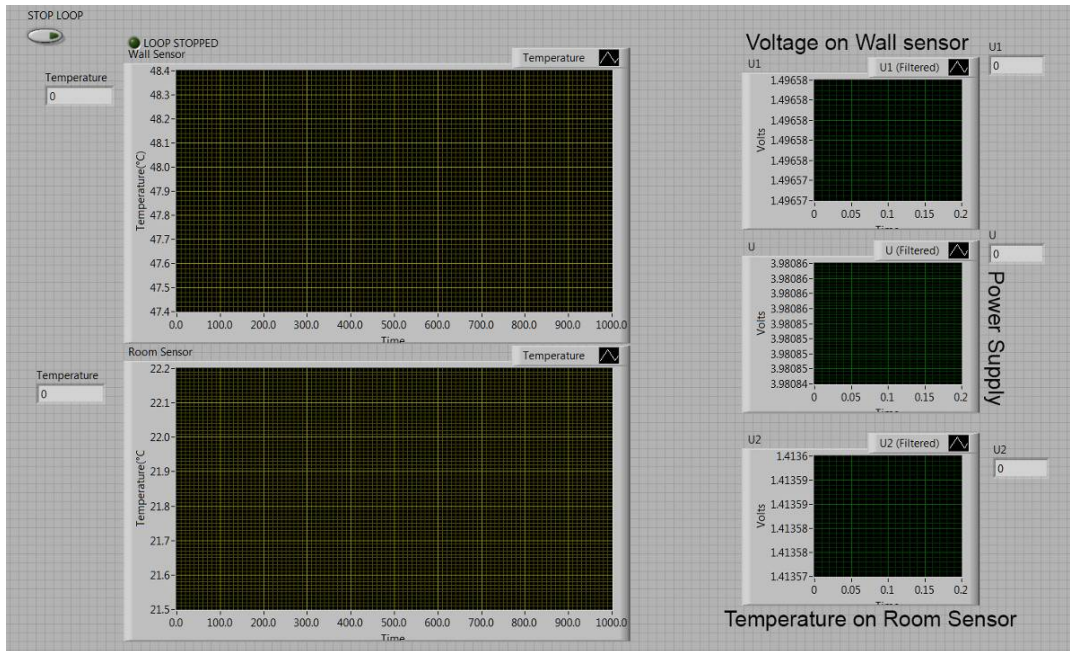


Figure A.6.1 Interface of the Labview Front Panel

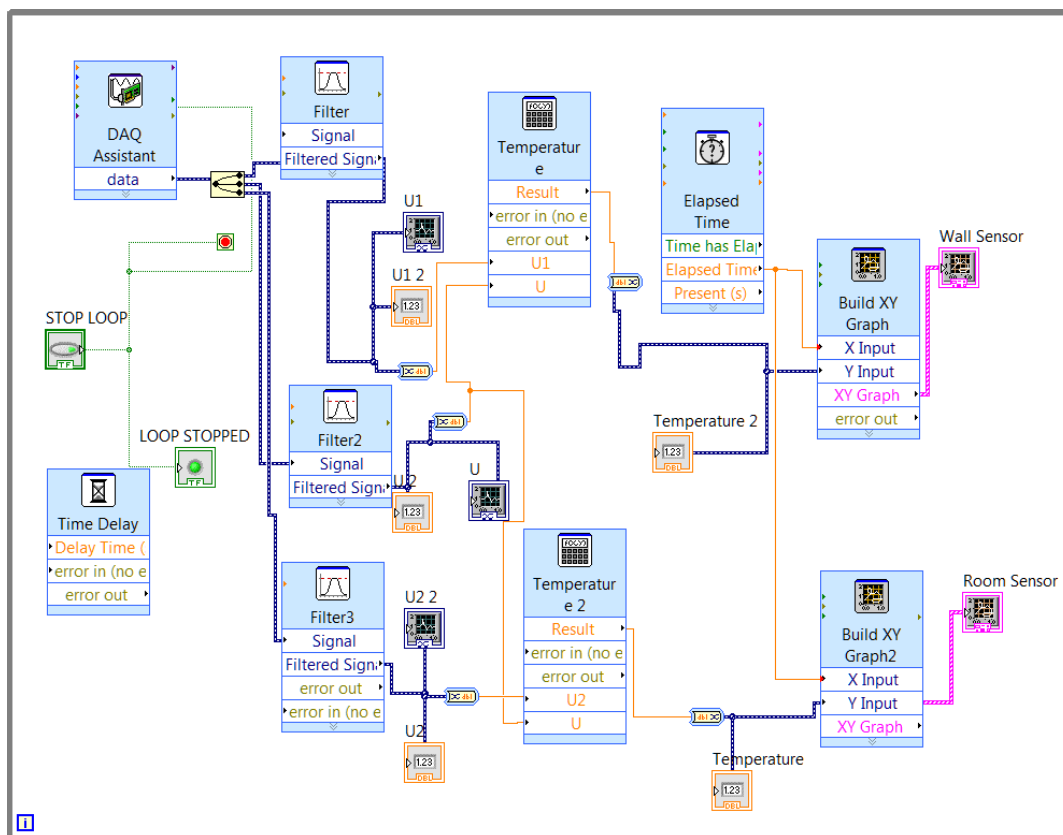


Figure A.6.2 Details of Labview Blocks Implemented

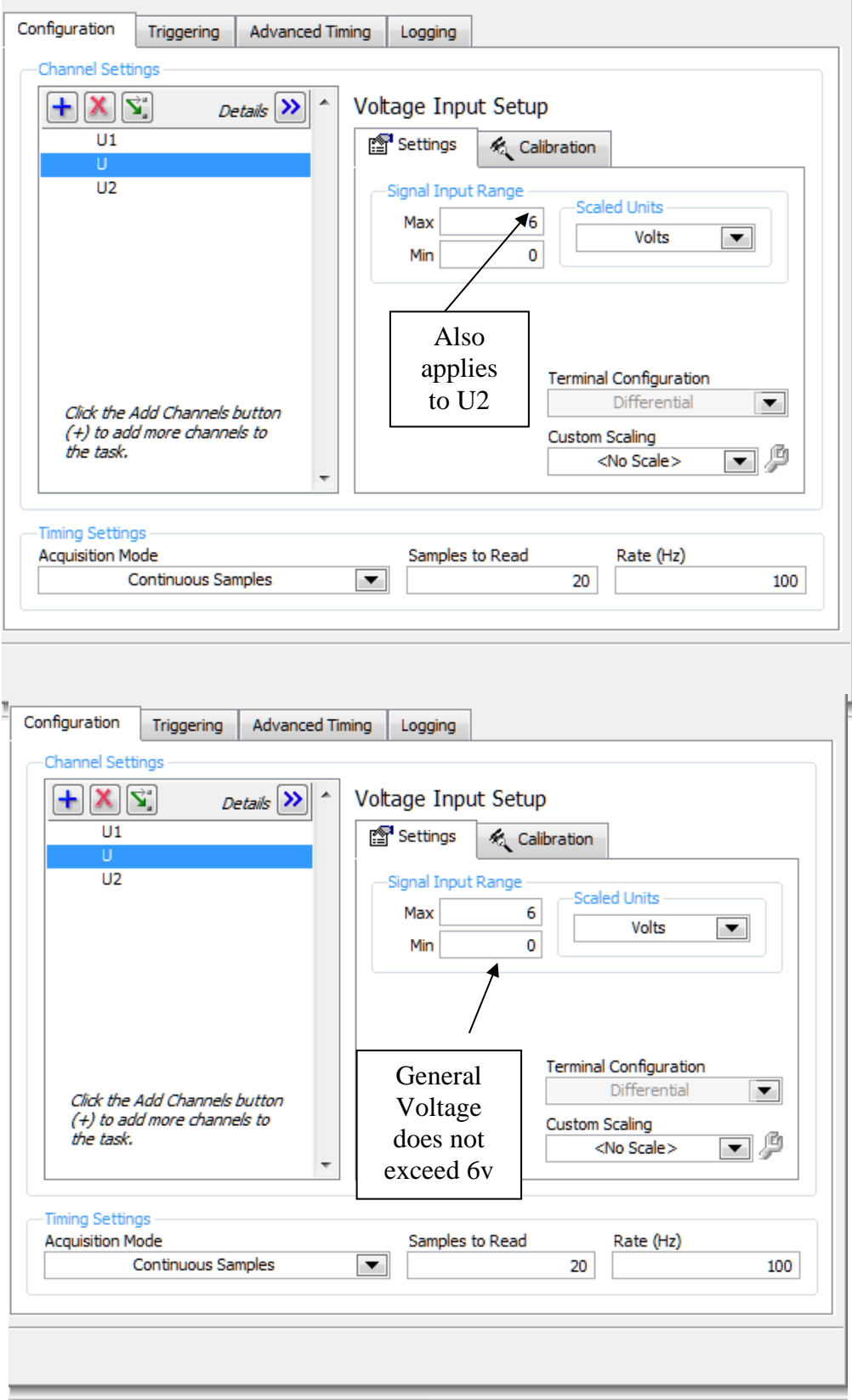


Figure A.6.3 DAQ Voltages Input Setup

## **A.2 SENSOR CALIBRATION DATA**

Calibration was under room temperature, which was 23.11°C. The margin of error for the wall and room sensor was 1-2%. The following two figures illustrate how the two RTD performed in the laboratory.

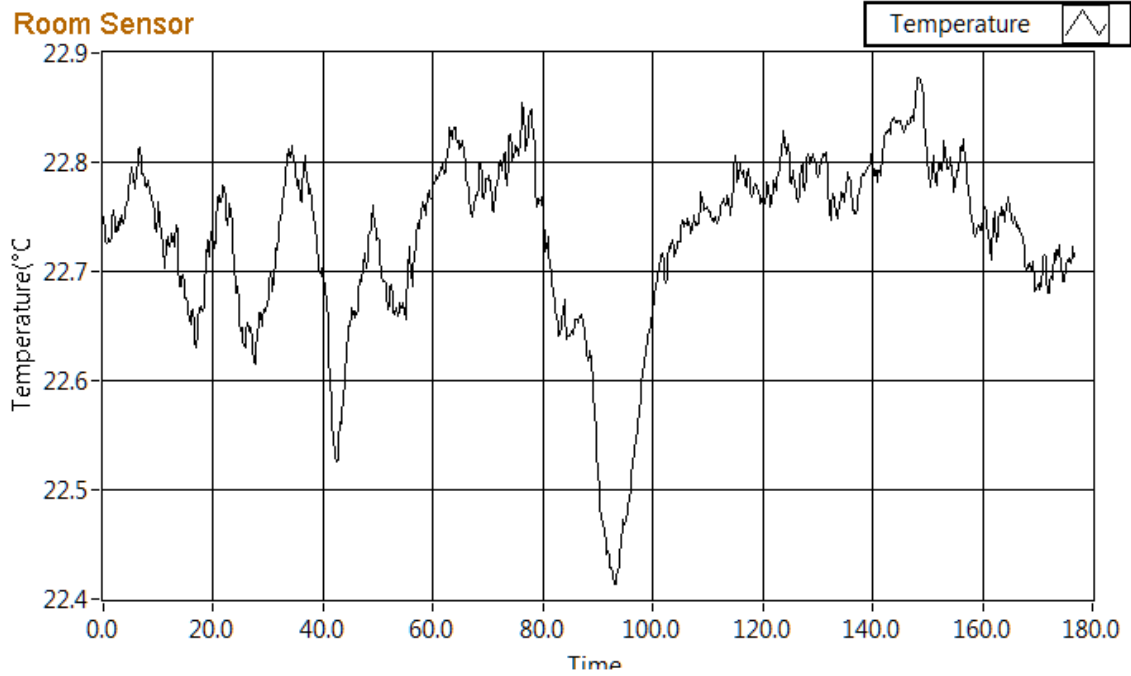


Figure A.6.4 Sensor Performances around Room Temperature

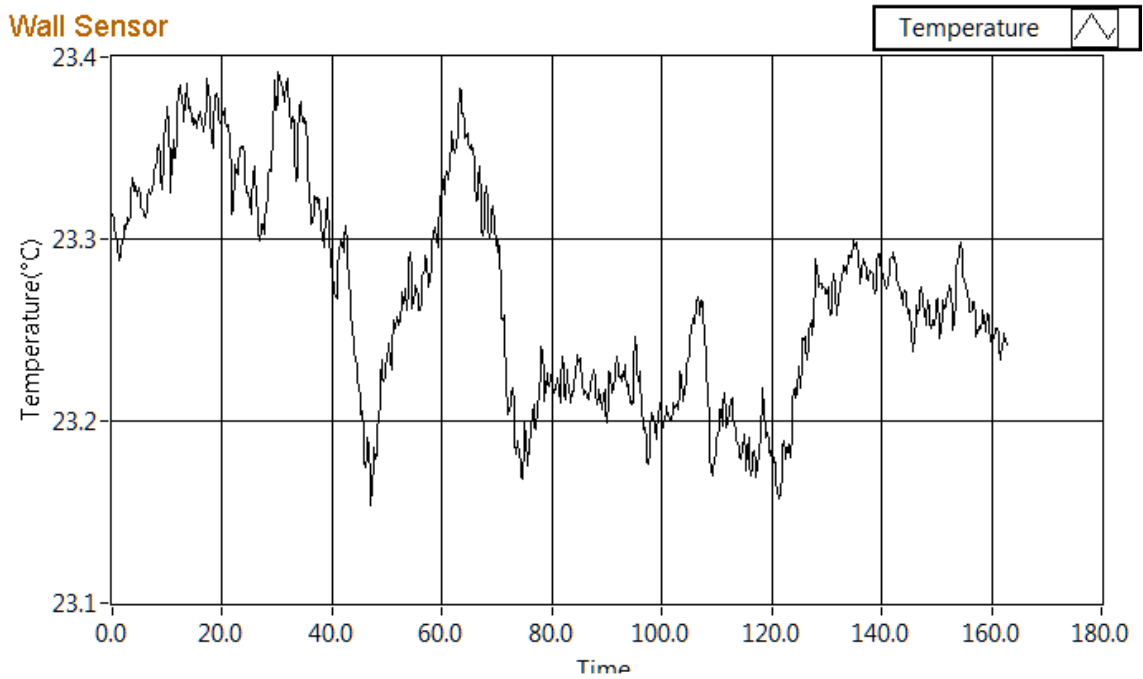


Figure A.6.5 Sensor Performances Attached on the Pipe Wall

APPENDIX B  
ESTIMATION OF THE CONVECTION COEFFICIENTS

**B.1 Convection Coefficient between the Air and Outer Wall**

As the pipe was horizontally placed in the laboratory under room temperature, the natural convection theory (in cylinder) was applied for finding the proper convection coefficient.

For air at 300K, the parameters of gases at the atmospheric pressure can be found from engineering handbook (1). For air at 23°C, thermal-expansion coefficient  $\beta = 1 / (273 + 23) = 0.0034$ . The corresponding air properties are listed accordingly in table A-1.

Table A-1 Air Properties at Atmospheric Pressure

<b>Density</b> $\rho = 1.177 \text{ kg} / \text{m}^3$	<b>Thermal Conductivity</b> $k_f = 0.02624 \text{ W} / (\text{m} \cdot \text{K})$
<b>Specific Heat</b> $c_p = 1005.7 \text{ J} / (\text{kg} \cdot \text{K})$	<b>Thermal Diffusivity</b> $\alpha = 0.22160 \times 10^{-4} \text{ m}^2 / \text{s}$
<b>Kinematic Viscosity</b> $\nu = 15.68 \times 10^{-6} \text{ m}^2 / \text{s}$	<b>Prandtl Number</b> $\text{Pr} = 0.708$

These parameters are associated with the important numbers required to calculate the natural heat convection coefficient between the air and outer pipe wall.

First, we find the Rayleigh number for the horizontal pipe, which was calculated by

$$Ra_D = \frac{g_x \beta (T_{air} - T_{out}) D^3}{\nu \alpha} = \frac{9.81 \times 0.0034 \times (23 - 10) \times 0.063}{(15.68 \times 10^{-6}) \times (0.2216 \times 10^{-4})} = 312030 \quad (\text{C-1})$$

For the horizontal pipe, the Churchill-Chu equation was applied, i.e.:

$$\overline{Nu}_D = \frac{\overline{h}_c D}{k_f} = \left\{ 0.6 + \frac{0.387 Ra_D^{1/6}}{\left[ 1 + \left( \frac{0.559}{Pr} \right)^{9/16} \right]^{8/27}} \right\}^2 \quad (C-2)$$

where  $\overline{Nu}_D$  is the Nusselt Number.

Rearranging equation (A-2) and substituting the Rayleigh Number, which leads to

$$\begin{aligned} \overline{h}_c &= \frac{k_f}{D} \left\{ 0.6 + \frac{0.387 Ra_D^{1/6}}{\left[ 1 + \left( \frac{0.559}{Pr} \right)^{9/16} \right]^{8/27}} \right\}^2 \\ &= \frac{0.02624}{0.063} \left\{ 0.6 + \frac{0.387 \times 312030^{1/6}}{\left[ 1 + \left( \frac{0.559}{0.708} \right)^{9/16} \right]^{8/27}} \right\}^2 = 4.39 \end{aligned} \quad (C-3)$$

According to the recommended range of the convection coefficient in [44], which is 10 to 200, through some trial and error the heat convection coefficient,  $h_c$ , is chosen to be 32.

## B.2 Convection Coefficient between the Water and the Inner wall

The convection coefficient between the water and the inner pipe wall differed from the other one calculated above since the convection inside the pipe was forced convection. Therefore, this requires another approach involving a few different numbers to reach the desired coefficient.

For the forced convection, it should follow the steps as follow:

First, it is necessary to determine Reynolds number.

The hydraulic diameter of the pipe  $D_H = d = 0.05m$ . The area of the pipe duct was

$$A = \frac{\pi d^2}{4} = \frac{\pi}{4} 0.05^2 = 1.96 \times 10^{-3} m^2 \quad (C-4)$$

The pump pressure equals 15L/min and the velocity of the water was calculated by

$$v = \frac{15 \times 10^{-3}}{1.96 \times 10^{-3} \times 60} = 0.127 m/s \quad (C-5)$$

Water density at 5°C is 1000kg/m<sup>3</sup>, dynamic viscosity is  $\mu = 1.52 \times 10^{-6} N - s / m^2$ . Therefore, the Reynolds number is:

$$Re = \frac{D_H v \rho}{\mu} = \frac{0.05 \times 0.127 \times 1000}{1.52 \times 10^{-3}} = 4178 > 4000 \quad (C-6)$$

Therefore, we know the fluid was considered turbulent.

Then, we determine the Nusselt number.

The fluid inside of the pipe was turbulent. As the specific heat  $c_p = 4202 j / kg$ , and thermal conductivity  $K_1 = 572 \times 10^{-3} W / (m \cdot k)$ , the Prandtl number was calculated by

$$Pr = \frac{\mu c_p}{K_1} = \frac{1.52 \times 10^{-3} \times 4202}{5.72 \times 10^{-3}} = 11.17 \quad (C-7)$$

Because

$$0.5 < Pr < 2000$$

$$3000 < Re < 5 \times 10^6$$

the Petukhove equation was applied, i.e., the Nusselt number was

$$Nu = \frac{\left(\frac{f}{8}\right)(Re-1000) Pr}{1 + 12.7\left(\frac{f}{8}\right)^{0.5}(Pr^{2/3}-1)} \quad (C-8)$$

where  $f = (0.79 \ln \text{Re} - 1.64)^{-2} = (0.79 \times \ln 4178 - 1.64)^{-2} = 0.0409$ . Substituting the Reynolds Number and the Prandtl Number, the Nusselt Number was

$$Nu = \frac{\left(\frac{0.0409}{8}\right)(4178 - 1000)11.17}{1 + 12.7\left(\frac{0.0409}{8}\right)^{0.5}(11.17^{2/3} - 1)} = 39.20$$

Therefore, the convection coefficient between the water and the inner wall was calculated by

$$h_1 = \frac{K_1}{D_H} Nu = \frac{0.572}{0.05} \times 39.20 = 448.448 \text{ W / (m} \cdot \text{K)} \quad (\text{C-9})$$

According to the recommended range of the convection coefficient in [44], which was from 50 to 10000, through some trial and error,  $h_1$  was chosen to be 450.

APPENDIX C  
ERROR ESTIMATION

**C.1 The Inference Error on the Temperature of Water from the Source of Error of the Sensor on the Outer Wall of the Pipe**

$$T_{water} = T_{out} + h_c D (T_{air} - T_{out}) \left( \frac{\ln \frac{D}{d}}{2\pi K} + \frac{1}{h_1 \pi D} \right)$$

$$T_{water} = \left( 1 - h_c D \left( \frac{\ln \frac{D}{d}}{2\pi K} + \frac{1}{h_1 \pi D} \right) \right) T_{out} + h_c D \left( \frac{\ln \frac{D}{d}}{2\pi K} + \frac{1}{h_1 \pi D} \right) T_{air}$$

$$dT_{water} = \left( 1 - h_c D \left( \frac{\ln \frac{D}{d}}{2\pi K} + \frac{1}{h_1 \pi D} \right) \right) dT_{out}$$

Given that  $h_c = 32$  ,  $h_1 = 450$  ,  $dT_{out} = 0.02$  ( i.e., the reading error of the RTD temperature sensor )

$dT_{water} = 0.019457$  . The margin of error for the sensor in the circulator approximately equals to 0.02.

**C.2 The Inference Error due to the Source of Error of the Temperature of the Air**

Consequently, we were able to estimate the measurement error caused by the air in the room through a similar approach.

$$T_{water} = T_{air} + h_c D (T_{air} - T_{out}) \left( \frac{\ln \frac{D}{d}}{2\pi K} + \frac{1}{h_1 \pi D} + \frac{1}{h_c \pi D} \right)$$

$$T_{water} = \left[ 1 + h_c D \left( \frac{\ln \frac{D}{d}}{2\pi K} + \frac{1}{h_1 \pi D} + \frac{1}{h_c \pi D} \right) \right] T_{air} - h_c D \left( \frac{\ln \frac{D}{d}}{2\pi K} + \frac{1}{h_1 \pi D} + \frac{1}{h_c \pi D} \right) T_{out}$$

$$dT_{water} = \left[ 1 + h_c D \left( \frac{\ln \frac{D}{d}}{2\pi K} + \frac{1}{h_1 \pi D} + \frac{1}{h_c \pi D} \right) \right] dT_{air}$$

Given that  $h_c = 32$ ,  $h_1 = 450$ ,  $dT_{air} = 0.03$

$dT_{water} = 0.0514$ . The error caused by the air temperature measurement is approximately equal to 0.05.